Homoclinic chaos in the Rössler model

Cite as: Chaos **30**, 113126 (2020); doi: 10.1063/5.0026188
Submitted: 21 August 2020 · Accepted: 21 October 2020 ·
Published Online: 10 November 2020

Semyon Malykh,[1] Yuliya Bakhanova,[1] Alexey Kazakov,[1,a)] Krishna Pusuluri,[2] and Andrey Shilnikov[3]

AFFILIATIONS

[1]National Research University Higher School of Economics, 25/12 Bolshaya Pecherskaya Ulitsa, 603155 Nizhny Novgorod, Russia
[2]Neuroscience Institute, Georgia State University, 100 Piedmont Ave. SE, Atlanta, Georgia 30303, USA
[3]Neuroscience Institute and Department of Mathematics and Statistics, Georgia State University, 100 Piedmont Ave. SE, Atlanta, Georgia 30303, USA

Note: This paper is part of the Focus Issue, Chaos: From Theory to Applications.
[a)]**Author to whom correspondence should be addressed:** kazakovdz@yandex.ru

ABSTRACT

We study the origin of homoclinic chaos in the classical 3D model proposed by Rössler in 1976. Of our particular interest are the convoluted bifurcations of the Shilnikov saddle-foci and how their synergy determines the global bifurcation unfolding of the model, along with transformations of its chaotic attractors. We apply two computational methods proposed, one based on interval maps and a symbolic approach specifically tailored to this model, to scrutinize homoclinic bifurcations, as well as to detect the regions of structurally stable and chaotic dynamics in the parameter space of the Rössler model.

This paper is dedicated to Otto Rössler who, being one of the pioneers in "chaosland," proposed several simple models with chaotic[1,2] and hyperchaotic[3] dynamics that became classics in the field of applied dynamical systems. The goal of our paper is to examine and articulate the pivotal role and interplay of two Shilnikov saddle-foci[4] in the famous 3D Rössler model as they shape the topology of the chaotic attractors such as spiral, screw-type without and with funnels, and homoclinic, as well as determine their metamorphoses, existence domains, and boundaries. Using the symbolic approach, we sweep its parameter space to identify periodicity/stability islands within chaoticity, as well as to examine in detail a tangled homoclinic unfolding that invisibly bounds the observable dynamics. The use of Poincaré return maps generated by solutions of the model lets us quantify the complexity of chaotic attractors and provides a universal framework for describing a rich multiplicity of homoclinic phenomena for which the classical Rössler model is notorious.

I. INTRODUCTION

The Rössler model[1,2] is a classic example of multi-faced deterministic chaos occurring in many low- and high-order systems. Its best known feature is the onset of chaotic dynamics due to a Shilnikov saddle-focus, that begins off with a period-doubling (PD) bifurcation cascade. The goal of this paper is to show how homoclinic bifurcations of two saddle-foci determine the organization and structure of chaotic attractors in the Rössler model. We consider its following representation:

$$\dot{x} = -y - z, \quad \dot{y} = x + ay, \quad \dot{z} = bx + z(x - c), \tag{1}$$

with x, y, z being the phase variables, and a, $c > 0$ being bifurcation parameters; we keep $b = 0.3$ fixed throughout this study. The convenience of the representation (1) is that one equilibrium (EQ) state, called O_1, of the model is always located at the origin $(0, 0, 0)$, while the coordinates of the second one O_2 are given by $(c - ab, b - c/a, -(b - c/a))$. One can notice that when $c = ab$, O_2 merges with O_1 and passes through it as a result of a transcritical saddle-node (SN) bifurcation. This is not the case in the other form of the Rössler model,[2]

$$\dot{x} = -y - z, \quad \dot{y} = x + ay, \quad \dot{z} = b + z(x - c), \tag{2}$$

where the location of neither equilibrium is fixed, and they emerge in the phase space through a generic saddle-node bifurcation. To become a saddle-focus, O_1 loses stability through a supercritical Andronov–Hopf (AH) bifurcation. Note that the transcritical saddle-node bifurcation makes another EQ O_2 a saddle-focus from the very beginning. It also undergoes an Andronov–Hopf bifurcation, though sub-critical after a saddle-periodic orbit collapses into O_2 to convert it into a repeller. We will proceed with this

discussion in the context of homoclinic bifurcations below. The AH bifurcation transforms the stable equilibrium O_1 into a saddle-focus of the (1,2)-type, i.e., with 1D stable and 2D unstable invariant manifolds due to single negative characteristic exponents $\lambda_1 < 0$, and a pair of complex-conjugated exponents $\lambda_{2,3} = \alpha \pm i\omega$ with a positive real part ($\alpha > 0$) [see insets in Fig. 6(b)]. Vice versa, the saddle-focus O_2 is of the (2,1)-type.

The vast majority of the papers on the onset and properties of chaos occurring in the Rössler model (1) are mainly focused on bifurcations related to the primary equilibrium state O_1, while leaving the role of the second saddle-focus O_2 in the shadow. In this paper, we will reveal the pivotal contribution of the latter, through homoclinic bifurcations, to the overall chaotic dynamics and its metamorphoses in this classical model.

Let us point out that in the parameter space of interesting dynamics for the model, the c-parameter is greater on the order of magnitude than the other parameters, a and b in the $(0, 1)$-range (see details in Refs. 5 and 6). This discrepancy in the parameter values implies that Eq. (1) possesses two-time scales with two slow (x, y)- and one fast z-phase variables. Moreover, the divergence of the vector field generated by Eq. (1) is estimated by $a + x - c$ or $a - c < 0$ around the origin O_1. This property makes the Rössler model strongly dissipative around the origin of the 3D phase space. However, that is not the case near the other equilibrium state O_2, where the divergence of the vector field is positive and small: $a(1 - b) \sim o(2)$. This observation partially explains a slow convergence of solutions to O_2 along its 2D stable manifold W^s as observed from Figs. 5(b_1)–5(c_1).

A. Period-doubling cascade to spiral chaos

Let us recap without excessive details what is well-known: the route to spiral chaos in the Rössler model through a cascade of period-doubling bifurcations. It is documented in Fig. 1 with fixed $c = 4.9$ as the a-parameter is increased. The supercritical AH-bifurcation makes O_1 the saddle-focus of type (1,2) and gives rise to the emergence of a stable periodic orbit (PO) [see Fig. 1(a)]. With a further increase in the a-parameter value, this PO loses the stability that is now inherited by periodic orbit of period-2 and next by an orbit of period-4 [Figs. 1(b) and 1(c)] through two initial period-doubling bifurcations. Further steps lead to the onset of longer stable POs through a Feigenbaum cascade toward the chaotic attractor discovered by Rössler in the model named after him.[1] Its interaction with a transverse cross-section in 3D would look like a Hénon attractor[7] with a recognizable parabola shape as one depicted in Fig. 3. Observe the shrinking hole around O_1 as depicted in Figs. 1(d) and 1(e) indicative that the saddle-focus remains isolated. At $a \approx 0.35$, the hole around it collapses, which eventually leads to the

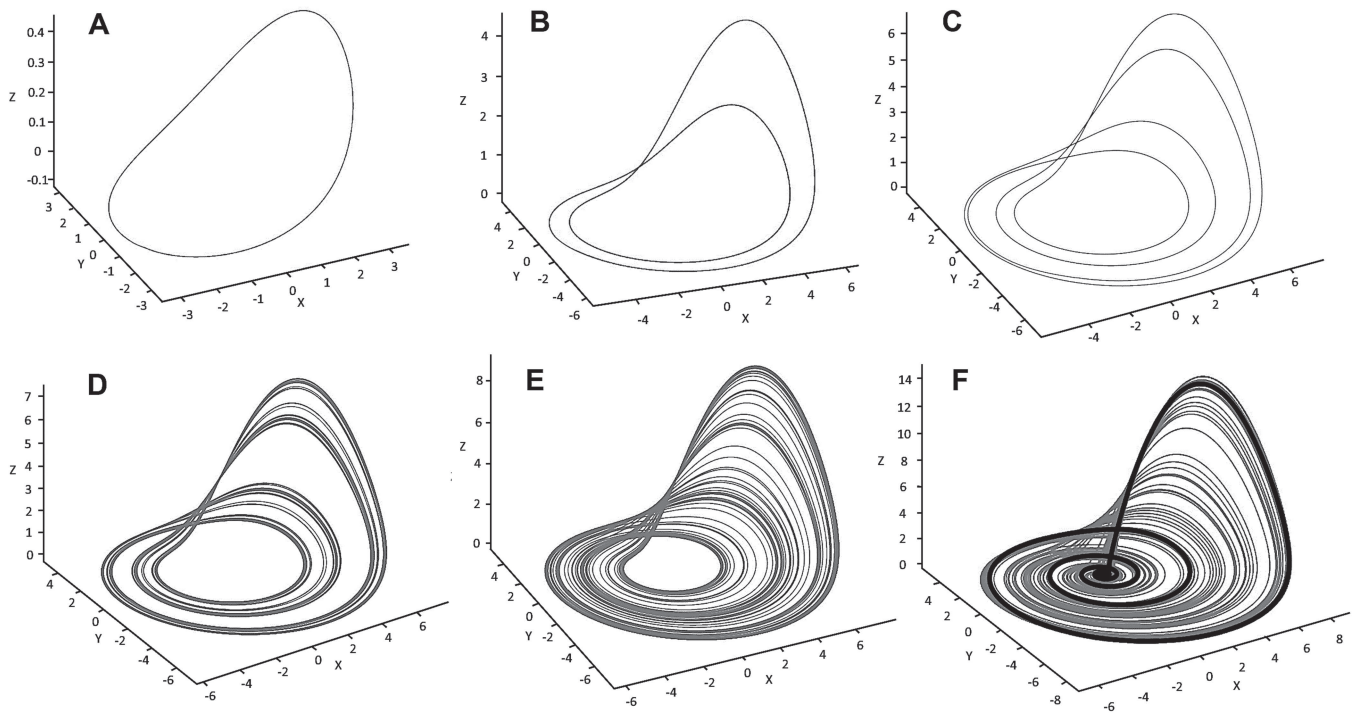

FIG. 1. Period-doubling bifurcations routing toward spiral chaos in the 3D phase space of the Rossler model on a pathway $c = 4.9$. (a) Stable periodic orbit (PO) at $a = 0.08$ is followed by a period-2 orbit at $a = 0.25$ in (b) and next by a stable period-4 obit at $a = 0.275$ in (c). Period-doubling chaotic attractors at $a = 0.28$ and 0.3 shown, respectively, in panels (d) and (e) morph into a spiral attractor with the Shilnikov homoclinic saddle-focus O_1 embedded at $a = 0.35$ (f), after the shrinking hole around it fully collapses.

formation of the primary homoclinic loop of O_1 [see Fig. 1(f)]. It is easy to argue that the Shilnikov bifurcation[4] causes a homoclinic explosion, giving rise to a hyperbolic subset containing countably many saddle POs inside the so-called *Shilnikov whirlpool*[8] formed nearby O_1 in the 3D phase space. It follows from the above arguments concerning the divergence $\sum_{i=1}^{3}\lambda_i = \lambda_1 + 2\alpha = a - c < 0$ of the vector field generated by Eq. (1) that $\lambda_1 + \alpha$ is negative too, i.e., the pair of complex-conjugate characteristic exponents $\lambda_{2,3} = \alpha \pm i\omega, \alpha >$ is located closer to the imaginary axis in the complex plane than $\lambda_1 < 0$. Such a location warrants the positiveness of the saddle value $-(\lambda_1 + \alpha)$ for the saddle-focus O of the (2,1)-type in *backward time* and, therefore, the fulfillment of the Shilnikov condition.[4] As saddle-periodic orbits near a homoclinic orbit of O remain saddle ones in the phase space of the system in forward time as well, this explains the cause and the nature of chaotic dynamics near the Shilnikov saddle-focus. A historic remark: the paper by Arnéodo *et al.*[9] was the first numerical evidence of strange attractors associated with the Shilnikov theorem in the Rössler model (1).

However, recall that a 3D dissipative system with the Shilnikov saddle-focus cannot produce a *purely chaotic* (or pseudohyperbolic) attractor[10,11] but a *quasiattractor*[12,13] instead (see more on pseudohyperbolic attractors and quasiattractors in Ref. 14). Homoclinic tangencies (literately stirred by the saddle-foci in the Rössler node) inside such a quasiattractor give rise to stable POs unpredictably emerging in the phase space through nearing saddle-node bifurcations and followed by period-doubling ones. To detect such stable POs and locate the corresponding stability windows in the biparametric sweeps, we propose and develop a symbolic approach combined with a phase space partition. With this approach, one can generate long binary sequences whose Lempel–Ziv (LZ) complexity[15] that, like the entropy, measures the degree of the repetitiveness of binary sequences. After being normalized over the sequence length (a few thousands of symbols in our case) its value indicates whether the given sequence corresponds to a periodic orbit (with a LZ-complexity value being almost zero) or to chaotic dynamics in the model. On the contrary, short binary sequences let us detect homoclinic bifurcations of saddle-foci in the phase and parameter spaces (see Sec. V).

The paper is organized as follows: first, we scan the parameter plane to detect the regions of regular and chaotic dynamics in the Rössler model. That is done by partitioning the 3D phase space and introducing a symbolic description for long-term solutions of Eq. (1). We next analyze the collected binary sequences to determine whether they are periodic or aperiodic and what the Lempel–Ziv complexity of chaotic sequences is. This fast and effective approach is an alternative to a less speedy method of Lyapunov diagrams (see details in Sec. II).

Section III is focused on the proposed algorithms for computationally devising return maps to examine the structure of the chaotic attractors in the model, and what makes them morph from spiral to multi-funnel shapes and how to detect such transitions in the parameter space. We argue that the number of critical points in such return maps can be used to adequately categorize homoclinic chaos in terms of spiral, screw-type, and multi-funnel attractors (see more details in Sec. III).

Next, we discuss an efficient approach to search for a small family of homoclinic bifurcations of the primary saddle-focus O_1 in biparametric sweeps. Having found these bifurcation curves, we employ the developed machinery of the interval return maps to give insights into a fine structure of particular objects—hubs where homoclinic orbits form the edges of the chaotic attractors in the phase space. In addition, Sec. III highlights how such return maps can predict the homoclinic bifurcations before they occur in the Rössler model.

Section IV is focused on the organization of a typical hub and how periodicity hubs shape the stability islands in the parameter space.

Section V discusses how the solution of the Rössler model becomes unbounded and what is the pivotal role of the secondary saddle-focus O_2 in shielding them from escaping to infinity. We reveal that the crisis is due to invisible homoclinic bifurcations of the saddle-focus O_2 and how this is related such that the Rössler model becomes no longer dissipative but expanding. Using the short symbolic dynamics, we find the first basic homoclinic bifurcations of O_2 and demonstrate how they arrange and demarcate the existence region of chaotic attractors in the given model.

In Sec. VI, we will speculate about a nested organization of homoclinic bifurcation curves in the interior of the primary U-shaped ones.

II. BIPARAMETRIC SWEEP WITH LZ COMPLEXITY AND DETERMINISTIC CHAOS PROSPECTOR

In the given section, we discuss the symbolic approach combined with the partition of the phase space to detect the regions of chaos and stability islands in the parameter space of the Rössler model (1). This is the first step before applying more dedicated tools for examining a variety of homoclinic bifurcations. We previously developed a symbolic toolkit, code-named deterministic chaos prospector running on graphics processing units (GPUs) to perform in-depth, high-resolution sweeps disclosing the fine organization of characteristic homoclinic and heteroclinic bifurcations and structures that have been universally observed in various Lorenz-like systems (see Refs. 16–20, and references therein). In addition to this approach capitalizing on sensitive dependence of chaos on parameter variations, the property of structural stability of regular dynamics can also be utilized to detect, fast and accurately, regions of simple and chaotic dynamics in a parameter space of the system in question.[21] The Z_2-symmetry is exploited to generate periodic or aperiodic binary sequences that may be associated, respectively, with simple or chaotic patterns of solutions of Lorenz-like systems. The application of the symbolic techniques for studies of neural dynamics in cell models and small neural networks is demonstrated in Refs. 22–24.

Our practical approach tailored specifically for homoclinic chaos in the Rössler model uses particular events when the z-variable reaches consequently its maximal values on the attractor. The binary sequence (k_n) representing a trajectory is computed as follows:

$$k_n = \begin{cases} 1, & \text{when } z_{max} > z_{\text{th}}, \\ 0, & \text{when } z_{max} \le z_{\text{th}}. \end{cases} \qquad z_{\text{th}} = 0.12(c - ab)/a. \tag{3}$$

Here, the z-threshold is set relative to the location of the saddle-focus O_2. The choice of partition is motivated by its simplicity and

may possibly be different, yet sufficient for our purpose. We note that various partitioning approaches may be employed for the same end result—effective detection of stability windows corresponding to regular and structurally stable dynamics in the parameter space of the Rössler model.

With this simple algorithm, we convert the maxima values of the z-variable into the binary symbols 0 and 1, based on some threshold value z_{th}. Biparametric sweeps such as those shown in Figs. 2, 6(a), and 8(a) are obtained by computing long trajectories starting from identical initial conditions (near the origin), and by skipping some initial transients, as two control parameters, c and a, are varied across a 5000 × 5000-size grid.

We use the fourth-order Runge–Kutta method with fixed step-size (GPU requirement) for numerical integration. The computation of trajectories across different parameter values is parallelized using GPUs. Data visualization is done using Python. Long-term system dynamics are analyzed by omitting the first 1000 symbols as transients, and processing the following 1000 symbols, to detect periodicity within the sequence. An overbar is used to represent periodic sequences such as $(010101\cdots)$ by simply $(\overline{01})$. Aperiodic strings representing chaotic trajectories are processed using the Lempel–Ziv (LZ) compression algorithm to measure their complexity.[15] As a string is continuously scanned, new words are added to the LZ vocabulary. The size of the vocabulary toward the end of the string, normalized with its length is used as the complexity measure, which is low for periodic sequences and high for chaotic ones. Chaotic dynamics are associated with the region painted in biparametric sweeps in the shades of gray, so greater LZ-complexity means darker gray, thus indicating higher instability. For trajectories mapped to periodic strings, the shift symmetry of the sequences must be considered. For example, depending on the length of the initial transient omitted, the same periodic orbit could be represented by either $\{\overline{01}\}$ or $\{\overline{10}\}$. We normalize such shift symmetric periodic sequences to the smallest binary-valued circular permutation. Thus, both $\{\overline{01}\}$ and $\{\overline{10}\}$ are normalized to $\{\overline{01}\}$, while the periodic sequences $\{\overline{011}\}$, $\{\overline{110}\}$, $\{\overline{101}\}$ are normalized to $\{\overline{011}\}$. Let us reiterate that we deliberately tailor this approach only to examine and detect chaos and stability islands due to saddle-node bifurcations in the parameter sweeps. As such, period-doubling bifurcations are beyond the scope of our consideration, even though the symbolic

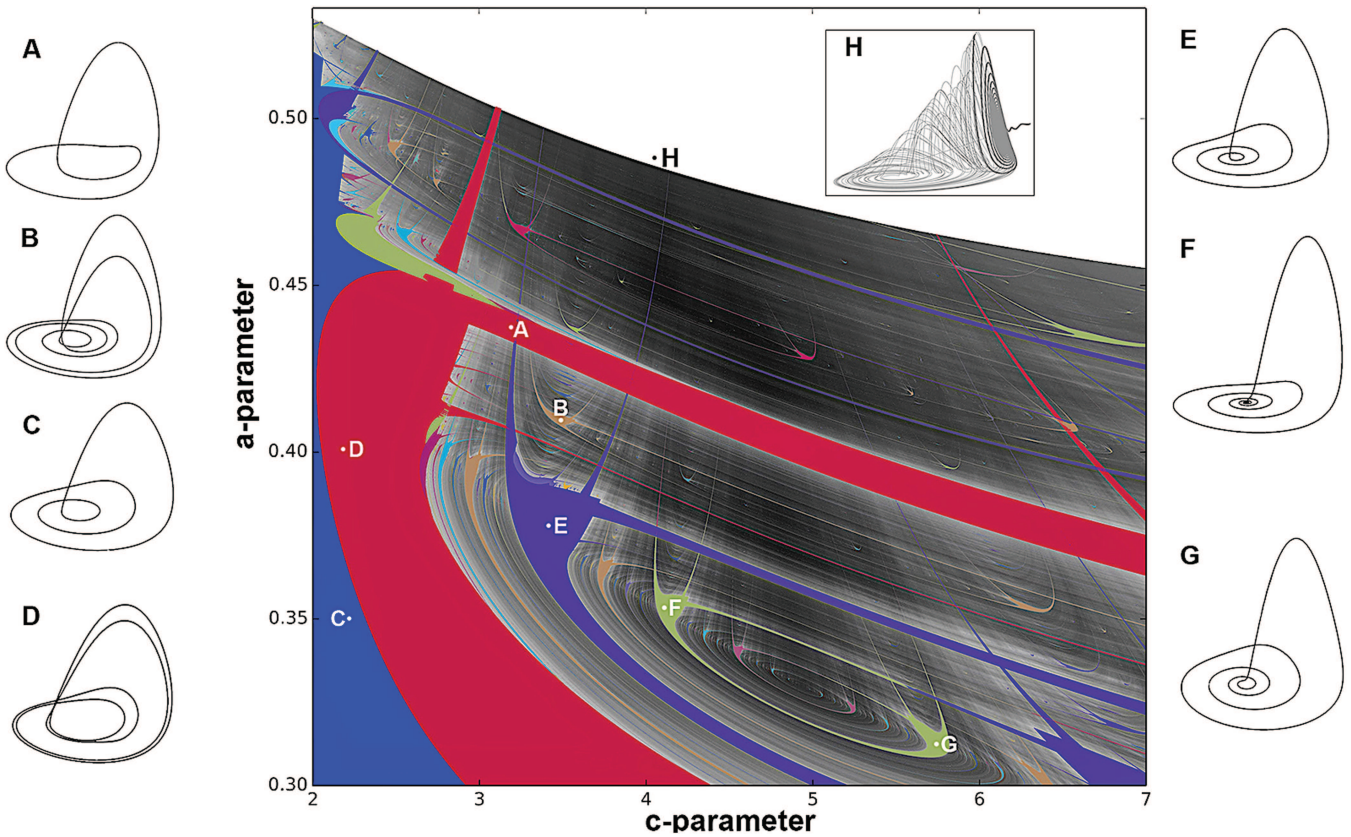

FIG. 2. The (c, a)-parameter [5000 × 5000]-resolution sweep of the Rössler model with the aid of the approach, combining deterministic chaos prospector and Lempel–Ziv-complexity, utilizing 1000-symbols long sequences, with first 1000 transients omitted. Shown in solid colors are multiple stability islands, including the so-called *shrimp*-shaped regions, hosting stable periodic orbits inside [some sampled in panels (a)–(g)], while the regions in the grayish color are associated with chaotic dynamics. (h) Solutions of (1) start escaping to infinity above some demarcation line (discussed in detail below).

approach can be further enhanced to detect such bifurcations as well.

In order to identify various stability windows in the parametric plane, we define a formal convergent power series P for the normalized periodic sequence $\{k_i\}_{i=p}^{q}$ given by

$$P = \sum_{i=p}^{q} \frac{k_i}{2^{q+1-i}}. \tag{4}$$

By construction, the P-value ranges between 0 and 1. The boundary values are set by the periodic sequences $\{\overline{0}\}$ and $\{\overline{1}\}$, respectively, for infinitely long sequences. Recall that here we employ $p = 1000$ and $q = 2000$. Parameter values that produce identical periodic orbits in their trajectories, result in identical sequences $\{k_i\}$ (after normalization of shift symmetry), and thus, have the same P values, which are then projected onto the biparametric sweep using a colormap. This colormap takes P values into 2^8 discrete bins of RGB-color values assigned from 0 through 1 for each channel of red, green, and blue colors in decreasing, random, and increasing order, respectively. The results of the sweep are demonstrated in Figs. 2, 6(a) and 15(a). Stability windows with distinct periodic orbits can be painted with different or same solid colors in the sweeps, while chaotic regions of structural instability are shown in gray; moreover, we re-emphasize the darker gray pixels are associated with more developed chaos in the Rössler model. For example, by construction [see Eq. (3)], the periodic orbits depicted in panels (a)–(f) in Fig. 2 are symbolically encoded as follows: $\{\overline{01}\}$, $\{\overline{0111}\}$, $\{\overline{001}\}$, $\{\overline{0101}\}$, $\{\overline{0001}\}$, and $\{\overline{00001}\}$. As such, their P-values evaluated through Eq. (4) will be different, except obviously for $\{\overline{01}\}$ and $\{\overline{0101}\}$.

To conclude this section, let us point out the mysterious demarcation line separating the region (here in white) where the solutions of Eq. (1) start escaping to infinity. The rest of the paper is basically dedicated to disclosing what this boundary is and how it influences the evolution of chaotic dynamics with underlying homoclinic bifurcations of both saddle-foci O_1 and O_2. We will proceed with the discussion of these results in detail below.

III. FROM SPIRAL TO SCREW-TYPE CHAOS WITH FUNNELS

The goal of this section is to demonstrate how chaotic attractors initially developed through period-doubling cascades evolve further, specifically as they approach the demarcation line in Fig. 2. We will demonstrate the role and applicability of Shilnikov saddle-focus bifurcation[4] and its unexpected developments[25] for the Rössler model. It was well-reported and discussed that chaotic attractors in the Rössler model could be of various shapes and complexity based on the number of nested sub-funnels (see Fig. 4), which increases as the demarcation line is approached from below. We note that Rössler himself was the first who introduced the classification of chaotic attractors in the model bearing his name (see Ref. 26). Alternatively, the transition after which the solutions become unbounded is often associated with the crisis occurring in the model on the demarcation line.[27] It is also well-known that the number of funnels can be effectively exposed with the use of return maps due to the strong contraction, as was done for the first time for the given system in Ref. 28. The use of such return maps happened to be instrumental in determining the topology of the attractors in question[29] and the complexity of saddle-periodic orbits embedded into an attractor. Depending on the number of branches in the corresponding maps, chaotic attractors can be categorized as spiral, screw, and multi-funnel attractors.[2,26,30]

A. Computational derivation of 1D return maps

Let us itemize our construction procedure for 1D return maps tailored for the Rössler attractors. First, the half-plane $\{y = 0, x \leq 0\}$ is chosen as a cross-section transverse to spiraling trajectories of (1) near O_1 to define a Poincaré return map $(x_{n+1}, z_{n+1}) = F(x_n, z_n)$ on a 2D cross-section, as illustrated in Fig. 3(a). Due to the strong contraction near the saddle-focus O_1, the intersection points of the chaotic attractor with the cross-section appear to lie on a 1D densely populated curve, as depicted by the inset of Fig. 3(a). Next, we parameterize this curve by the Lagrange polynomial $z(x)$ using four points: the first point $(0, 0)$ corresponds to the saddle-focus O_1, the second point $(x_{min}, z(x_{min}))$ is a point with the minimal x-coordinate belonging to the attractor, and two middle points on it. Finally, we evaluate the corresponding return map $x_{n+1} = F(x_n, z(x_n))$ using 5000 points populating the interval $[x_{min}, 0]$. The resulting 1D map for the chaotic attractor embedded with the primary homoclinic orbit to the saddle-focus O_1 is presented in Fig. 3(b).

By construction, such a map has a few pivotal features: (a) it inherits a unimodal shape (with a single point) from a period-doubling cascade; (b) $0 = F(0)$ is a repelling fixed point (FP) representing the saddle-focus O_1; (c) the far-right critical point always touches the x_n-axis; (d) in the homoclinic case, the forward iterates of the critical point terminate at the repelling FP, while its backward iterations converge to it along the right increasing branch of the map [corresponding to the homoclinic loop in Fig. 3(a)]; and (e) otherwise, the forward iterates of the critical point cannot reach the FP as the left branch(es) and all local maxima are lowered below, prior to or after the homoclinic bifurcation. This can be interpreted that the saddle-focus O_1 becomes (temporarily) isolated from the chaotic attractor in both super- and sub-critical homoclinic cases, like the one depicted in Fig. 1(e).

Having developed the proposed map-based methodology, we can differentiate chaotic attractors in the Rössler model by the complexity of their funnels following the approach that was originally proposed in Refs. 2, 26, 29, and 30. In particular, whenever the corresponding return map has only two branches, the attractor is called spiral [see Fig. 4(a)]. It can be homoclinic if the critical point is taken right into the FP at O, like in Fig. 3(b), or not [when the left branch is not as high as the right one; see Fig. 4(a_2)]. The chaotic attractor is called of screw-type when the map gains an additional (third) branch [see Fig. 4(b_2)], and multi-funnel if the map has four or more branches [see Fig. 4(c_2)]. We re-emphasize that either attractors becomes a homoclinic one only if the images (forward iterations) of the far-right critical point on the x_n-axis ends up at the repelling FP at the origin.

In conclusion, we would like to say that the proposed return-map approach helps differentiate the chaotic attractors by the complexity of the funnels and can also predict and accurately verify

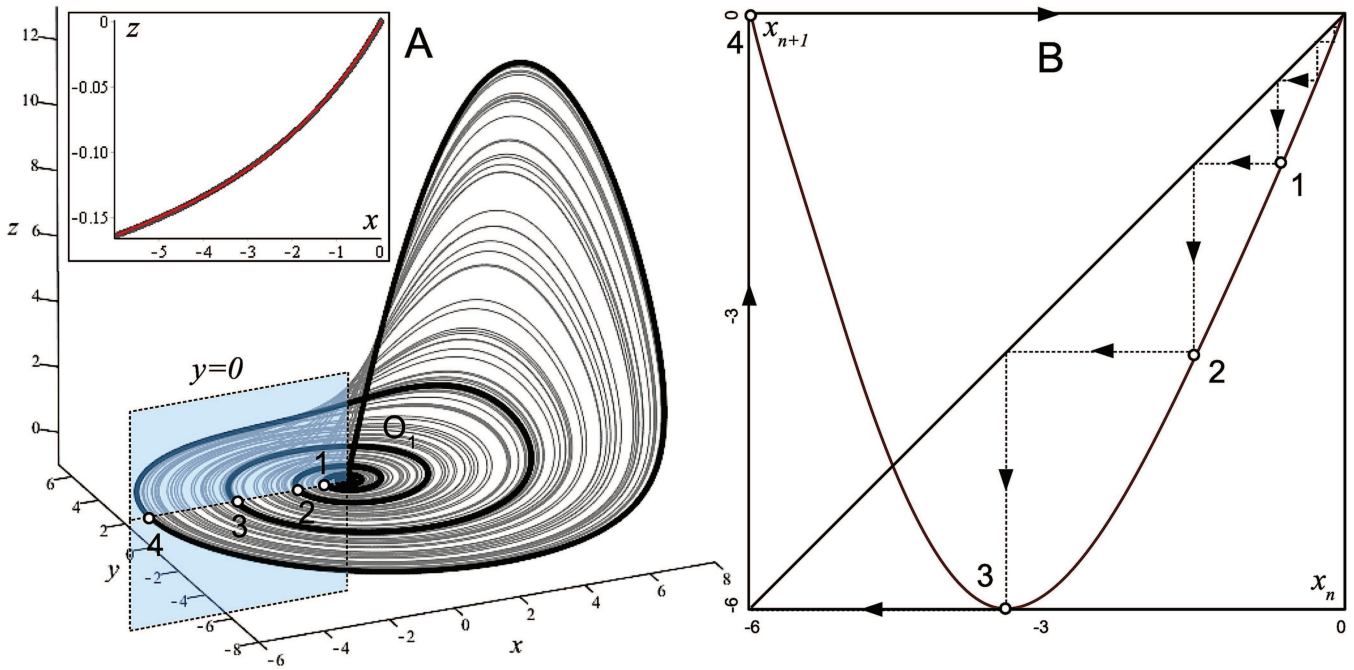

FIG. 3. (a) Spiral attractor ($c = 4.93$, $a = 0.33$), superimposed with the primary homoclinic orbit of the saddle-focus O_1, and its intersection points with a 2D cross section (a blue plane) given by $y = 0$ and $x \leq 0$. (b) Computationally interpolated return map $F : x_n \to x_{n+1}$ of an interval spanning from O_1 through the edge of the chaotic attractor in the above 2D cross section. Forward/backward iterations {1, 2, 3, 4} of the critical point on the x_n-axis, approach/converge, respectively, to the repelling fixed point (FP) at the origin O, corresponding to the homoclinic orbit of O_1 in (a).

whether any homoclinic loop of the saddle-focus O_1 occurs or not for the given parameter values.

B. Funnels stirred by saddle-focus O_2

Let us highlight an invisible role of the second saddle-focus O_2 implicitly regulating the formation of funnels in the chaotic attractors in the Rössler model. Recall that this saddle-focus is of the (2,1)-type. Its 2D manifold W^s, locally dividing the 3D phase space near O_2, forms an umbrella shielding the domain of the chaotic attractor that prevents nearby solutions from escaping to infinity along 1D unstable separatrix W^{u-} of O_2 [Fig. 2(h)]; the other 1D separatrix W^{u+} ends up in the attractor [Fig. 5(b_1)].

Figures 5(b_1) and 5(c_1) illustrate the role of O_2 in the funnel formation. Both depict the chaotic attractor in the phase space as the demarcation line in Fig. 2 is approached from below in the parameter space. The attractor is superimposed with a local portion of the stable manifold (shown in blue) of the saddle-focus O_2; blue spirals also reveal the slow rate of the convergence of orbits to O_2 on its the 2D stable manifold, which is indicative of the closeness of the corresponding characteristic exponents to the imaginary axis. The (orange) spiraling line is composed of a large number of intersection points of the chaotic attractor with a transverse cross section ($y = -2$ or -4). One can notice that the closer the attractor gets to the stable manifold of O_2, the more it becomes wrapped around W^{u+}. Figure 5(b_1) also shows W^{u+} unidirectionally connecting O_2 with O_1. This explains the origin of the funnels observed in the chaotic attractors in the Rössler model, which are reflected in adding new branches in the return maps [Figs. 4(a_2)–4(c_2)].

IV. HOMOCLINICS, HUBS, AND SHRIMPS

Here, we will discuss phenomena that underlie a multiplicity of periodicity windows, which are well-seen in Fig. 2. It is very well-known (see, e.g., Refs. 4, 8, and 33–35) that there are countably many saddle POs near the Shilnikov homoclinic saddle-focus in the phase space. The stable and unstable manifolds of such saddle POs can cross each other transversally or become tangent; moreover, systems with such homoclinic tangencies fill in open regions of the parameter space. Specifically, homoclinic tangencies give rise to the emergency of stable POs in the 3D phase space through forthcoming saddle-node bifurcations[13,36,37] [see a few stable POs sampled in Figs. 2(a)–2(g)]. One can see from the sweep in Fig. 2 that the parameter space of the Rössler model, which is mostly populated by chaotic dynamics, also embeds solid-color regions called periodicity windows or stability islands that are populated by stable periodic orbits. Strange attractors of such intermediate nature, where hyperbolic (chaotic) subsets coexist with stable POs therein in the phase space for same or close parameter values, were termed *quasiattractors* by Afraimovich and Shilnikov[12] (see also Ref. 13). Below, we will elaborate on the bifurcation unfolding of those self-similar

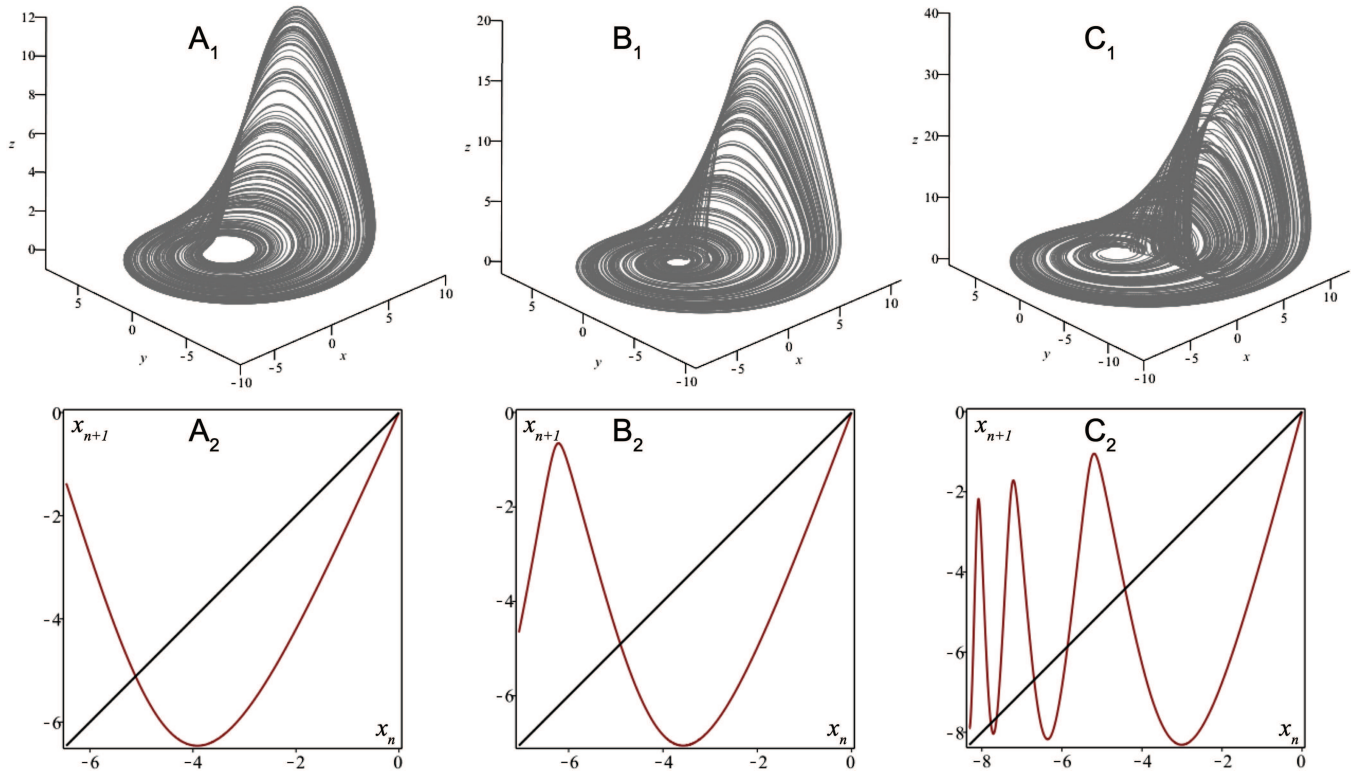

FIG. 4. Changes in the topology of the chaotic attractor in the Rössler model as it shifts closer to the secondary saddle-focus O_2 along the pathway at $c = 5.5$. (a_1) The spiral attractor at $a = 0.3$ and (a_2) the corresponding 1D unimodal map; (b_1) a screw-like attractor at $a = 0.355$ and (b_2) the corresponding return map with two critical points; and (c_1) multi-funnel attractor at $a = 0.455$ and (c_2) the associated 1D map with multiple critical points. As the saddle-focus O_1 being isolated from the non-homoclinic chaotic attractor in each phase projection, all maxima in these maps are located below the repelling FP at O representing O_1.

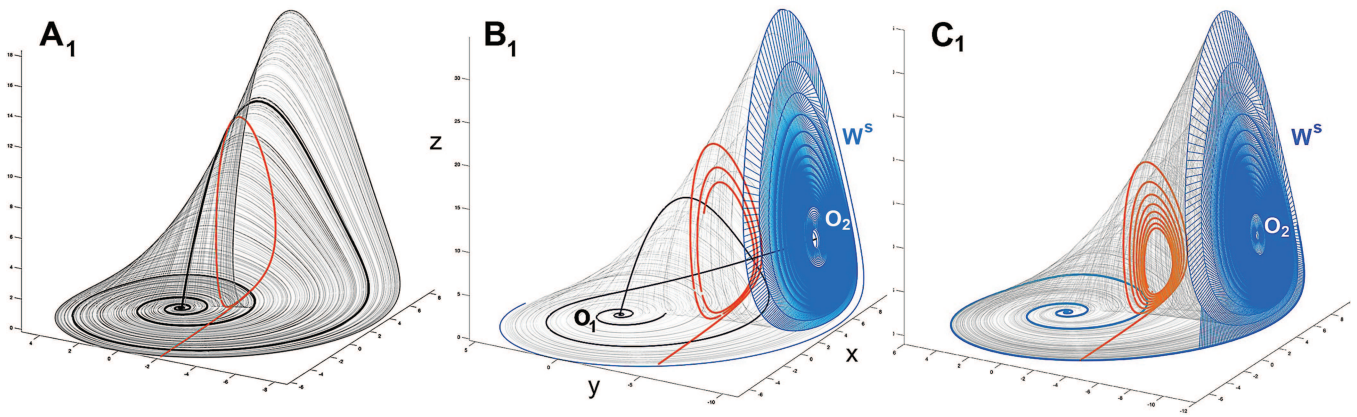

FIG. 5. Chaotic attractors (gray color) morphing from (a_1) the spiral one with a homoclinic orbit of the saddle-focus O_1 at $(c,\ a) \simeq (4.822,\ 0.38)$ to the attractor with emerging funnels at $(4.615, 0.468)$ with a unidirectional heteroclinic connection from O_2 to O_1 in (b_1), and through the multi-funnel attractor at $(4.652,\ 0.4775)$ in (c_1). The spirals in the orange color reveal the ways the attractors hit some transverse cross sections ($y = -2, -4$) in the phase space. Blue lines in panels (b_1) and (c_1) represent the location of the 2D stable manifold W^s of the saddle-focus O_2 that makes the chaotic attractor wraps around the left unstable separatrix W^{u+} of O_2 the more, the closer it shifts to the secondary saddle-focus, whose manifold W^s shields the solutions of Eq. (1) from escaping to infinity [see Fig. 2(h)].

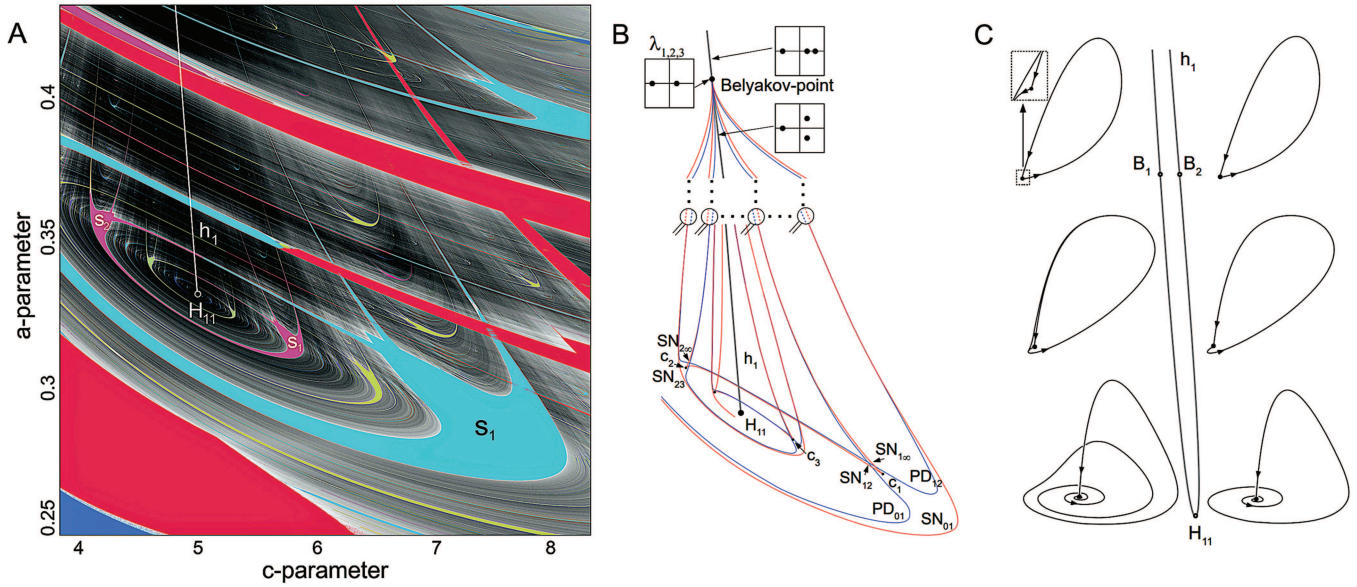

FIG. 6. (a) Fragment of the biparametric sweep. Solid, colored regions S_1, S_2, S_3, ... are associated with stability islands corresponding to the attracting POs, emerging within chaosland painted with the grayish colors. The line h_1 with the end-point H_{11} corresponds to the primary homoclinic bifurcation of the saddle-focus O_1 [see Fig. 1(f)]. (b) Sketch of the self-similar bifurcation diagram near h_1. Outer borderline of a shrimp-shaped region S_i is due to saddle-node (SN) bifurcation curves $SN_{i-1,i}$ (in red) bridging with a successful one S_{i-1} and originating from the Belyakov codimension-2 point corresponding to a homoclinic saddle with double real characteristic exponents $\lambda_2 = \lambda_3 > 0$. Inner demarcation line of S_i is due to period-doubling (PD) bifurcations (blue lines): the first curve $PD_{i-1,i}$ connecting successive S_i and S_{i-1} regions also starts off the Belyakov point, and so forth. Note the cusps on SN-curves such that $SN_{i,i+1}$ links S_i and S_{i+1} islands, while $SN_{i,\infty}$ terminates at the Belyakov point. (c) Evolutions of single and double homoclinic orbits to O_1 transitioning from a saddle to a saddle-focus and back along the U-shaped bifurcation curve h_1, with the tip H_{11} being a turning point (simulations due to MatCont[31,32]).

stability windows, labeled by S_i in Fig. 6(a), that have the specific shrimp-shape.

The gray curve h_1 in Figs. 6(a), 8(a), and 15 corresponds to the primary homoclinic bifurcation of the saddle-focus equilibrium O_1. The paper[28] was the first study carrying out a detailed analysis of the self-similar organization of stability windows emerging near this curve in the parameter plane. Its bifurcation unfolding is outlined in Fig. 2(b), following the original paper. Specifically, its authors showed that each periodicity window is bordered by a saddle-node bifurcation curve $SN_{i-1,i}$ on one side such that a stable PO emerges upon inward-crossing of this curve, along with a saddle one. The stable orbit undergoes a cascade of period-doubling bifurcations. Curves $PD_{i-1,i}$ and $PD_{i,i+1}$ in Fig. 2(b) represent the first bifurcations in such cascades.

Note a cusp point c_i inside each shrimp-like stability window S_i, where the sub-criticality of SN-bifurcations changes. Due to such cusps, the dynamics inside the shrimp-shaped regions can be bistable. As was established in Ref. 28 that one curve, SN_{12}, originating from the cusp c_1 inside the shrimp S_1 connects to a subsequent cusp c_2 within the other shrimp S_2 containing the same stable POs. Furthermore, the bifurcation curve, SN_{23}, forming the left-bottom boundary of S_2 coalesces with the SN-curve representing the right-bottom boundary of the third shrimp S_3, and so forth. Due to such connectivity, these stability windows, alternating with regions of chaotic dynamics, appear as some nested spirals winding around what is code-named *periodicity hubs*,[39] associated with a faux codimension-2 bifurcation, if any. Note that this interesting structure was first reported in the original paper.[28] Hubs in the Rössler model and other systems with homoclinic saddle-foci were numerically studied using Lyapunov exponents in various diverse applications (for example, see Refs. 39–41, and references therein).

It is interesting to note that, apparently, the SN and PD bifurcation curves edging the shrimp-shaped windows near the homoclinic bifurcation curve all branch out from a specific codimension-2 point corresponding to a transition from a homoclinic saddle to a homoclinic saddle-focus. In virtue of the Belyakov theorem,[42] such a point gives rise to a countable number of SN-curves and double homoclinic bifurcation curves accumulating to it in the parameter plane on the saddle-focus side. It is shown in Ref. 45, with the aid of the numerical parameter-continuation approach, that this is the case for the tri-trophic food chain model with similar dynamical and bifurcation properties. As for the Rossler model, it is shown numerically in Ref. 38 that several SN and PD bifurcation curves do originate from the Belyakov point, as sketched in the top chart in Fig. 2(b).

In the given context, the Belyakov point stands for the codimension-2 bifurcation describing the transition from a homoclinic saddle to the Shilnikov saddle-focus. In addition, there are two other Belyakov points relating different codimension-2 homoclinic bifurcations: a resonant saddle-focus with a zero saddle value,[43] and the so-called Shilnikov–Hopf bifurcation through which

a saddle-periodic orbit collapses into a homoclinic saddle-focus through a sub-critical Andronov–Hopf bifurcation.[44]

Another interesting result reported in Refs. 38 and 45 is that all primary and secondary homoclinic bifurcation curves in both food chain and Rössler models have the specific U-shaped form in the parameter space. Due to strong contraction and slow-fast dynamics, two extremely close (the distance between them 10^{-10}) branches of the curves h_1 and others look like a single one [see a schematic diagram shown in Fig. 2(c)]. The fold or turning point H_{11} on h_1 represents the primary periodicity hub. Observe that the left branch of h_1 corresponds to double homoclinic orbits, in contrast to ones associated with the right branch.[38,45]

A. Primary homoclinic curves and periodicity hubs

It was shown in Ref. 41 that on the left from the primary homoclinic bifurcation curve h_1, there exist several subsequent ones h_i, $i \in [2, 3, \ldots]$ corresponding to double, triple, and longer homoclinic orbits [see Figs. 6(a) and 8(a)]. All these curves are of the U-shaped form with fold points at the corresponding periodicity hubs H_{ii}. In Fig. 8, such curves can be typically detected and computed using numerical continuation toolkits such as AUTO or MatCont. We stress that in the parameter regions between curves h_i and h_{i+1}, there are *no* other homoclinics to the saddle-focus O_1. This fact can be verified using the proposed return maps. Let us consider three particular points in the (c, a)-bifurcation diagram: the points A (4.6, 0.35) and C (5.2, 0.35) are chosen on the opposite sides from the bifurcation curve h_1 of the primary homoclinics of O_1, whereas the point B (4.89, 0.35) is placed very close to it [see Fig. 8(a)]. At the point A, as well as the point C, the images of the local maximum in the return map are below the repelling FP at the origin O, which is interpreted as the saddle-focus O_1 being isolated, outside of the chaotic attractor [see Figs. 7(a) and 7(c)]. This is not the case for the point B, where the local maximum is taken to the FP O after a single iterate [see Fig. 7(b)], which indicates that the saddle-focus O_1 is the intrinsic component of this homoclinic attractor, in contrast to the other two cases.

In this work, we applied an alternative approach for finding the curves h_i which is better suited for systems with various saddles of the (1,2)-type.[46,47] Our search strategy is based on the fact that a homoclinic attractor (following its mathematical definition introduced in Refs. 48 and 49) embeds homoclinic loops of O_1, whose simulated trajectories will come close by the saddle-focus O_1 eventually. By performing one- and two-parameter sweeps, we estimate the distance to O_1 from a long typical trajectory on the attractor. Whenever the distance becomes less than some threshold value d_{tr} (we use $d_{tr} = 0.001$), the saddle-focus O_1 (together with its homoclinic orbit) is meant to belong to the attractor.

Figures 8(b) and 8(c) are de facto demonstrations of the efficiency of the described approach for two one-parameter pathways: P_1Q_1 given by $\{a = 0.45;\ 4 \le c \le 5\}$ and P_2Q_2 given by $\{a = -1/60c + 0.55;\ 3.3 \le c \le 4.8\}$. Along the first pathway P_1Q_1, the distance graph has two local minima below the threshold: the first minimum corresponds to the homoclinic bifurcation value on h_2 and the second one occurs on the curve h_1. Along the second pathway P_2Q_2, there are four such local minima in the graph, the distance plotted against the c-parameter, corresponding to the curves h_4, h_3, h_2, and h_1.

Next, let us describe the curves m_1, m_2, and m_3 that are also superimposed with the sweep in Fig. 8(a). These curves were found using the return maps, namely, below m_j, the return maps consist of j connected parabolas, whereas above it, the maps gain the additional $(j+1)$th branch, as seen in Figs. 4(a_2) and 4(b_2) depicting the 1D return maps below and above the m_1-curve, respectively.[47] When the image of the new local maximum (on the far-left branch) on the m_j-curve is the repelling FP O, this corresponds to the occurrence of the j-round homoclinic orbit to the saddle-focus O_1. For example, see the map associated with the hub H_{11} on the primary h_1-curve through which the curve m_1 passes in Fig. 3.

Figure 9 illustrates the homoclinic phenomena in other found hubs H_{22}, H_{33}, and H_{44}. The first row in this figure presents the

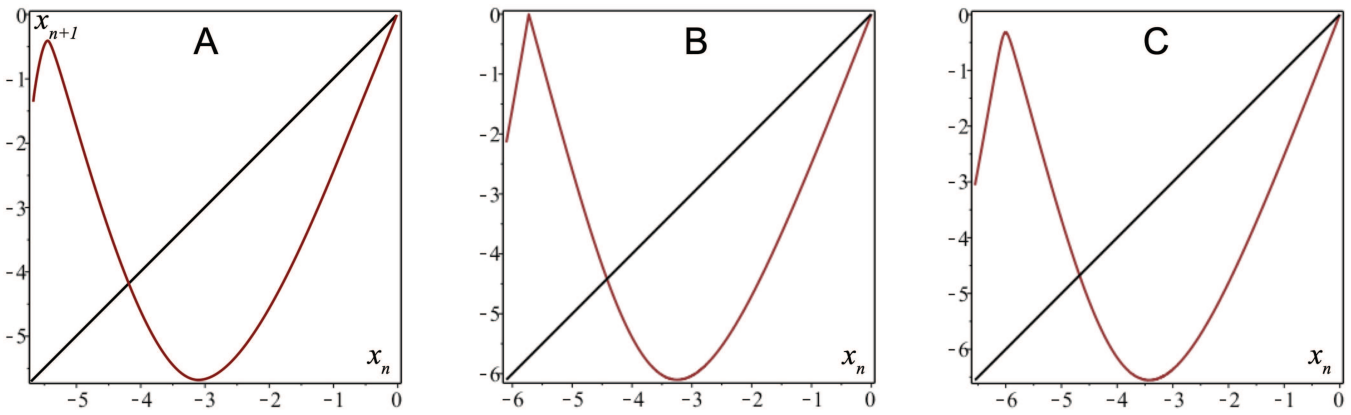

FIG. 7. 1D return map generated by the trajectories of the chaotic attractors sampled along the pathway $a = 0.35$ near the primary bifurcation curve h_1: (a) the local minimum is below the repelling FP at the origin at $c = 4.6$ (on the left next to h_1), (b) the local minimum is taken to the origin after one iterate at $c = 4.89$ (on h_1), and (c) the map at $c = 5.2$ (on the right next to h_1) is similar to the one in panel (a).

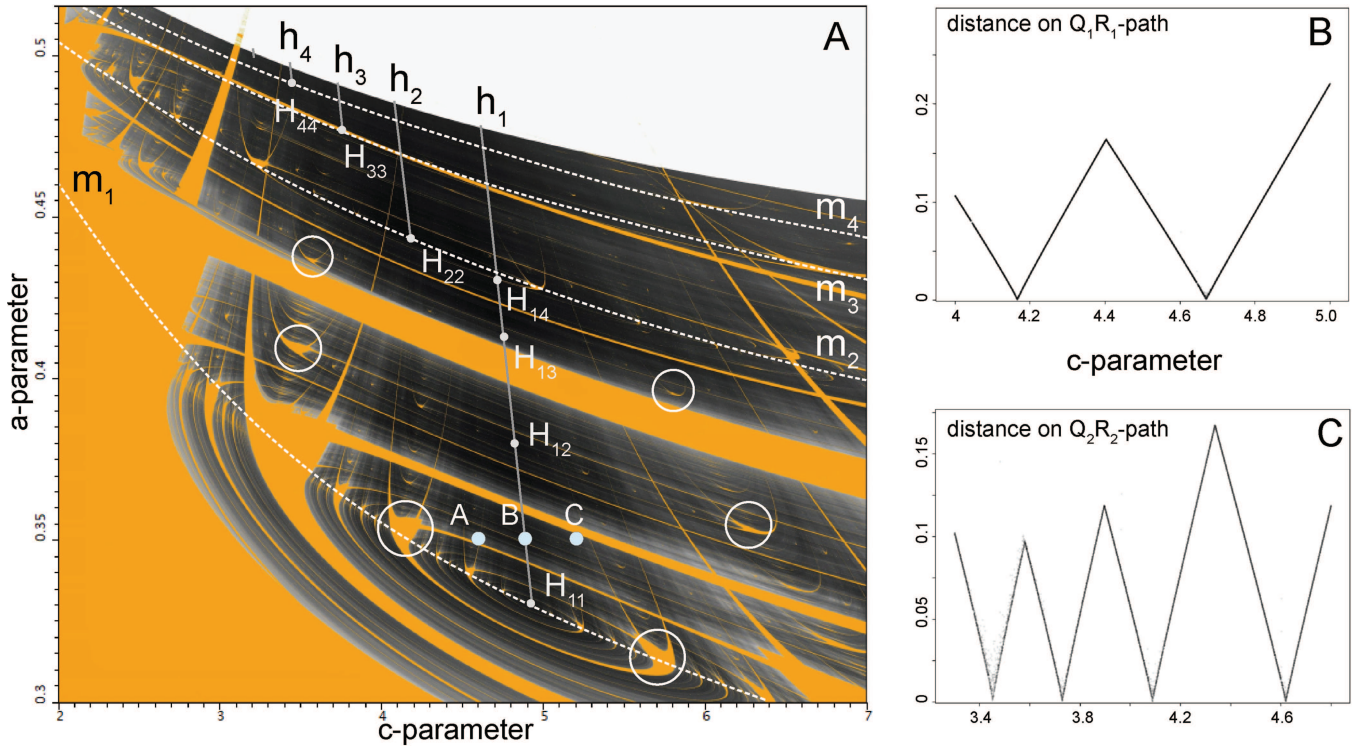

FIG. 8. (a) Biparametric sweep with superimposed curves: m_i, $(i = 1, \ldots, 4)$ corresponding to the emerging $(i+1)$th branches and new critical points in the return maps (see examples in Figs. 4 and 9); specifically, above m_1, the spiral attractor transforms into a screw-type.[26,29,38] Curves h_i with tipping points H_{ii} on m_i stand for homoclinic bifurcations of O_1 and primary periodicity hubs H_{ii}, respectively. Shrimp-like windows (some circled) form what looks like nested spirals around the periodicity hubs. (b) and (c) The distance between the saddle-focus O_1 and the chaotic attractors on the P_1Q_1- and P_2Q_2-pathways, respectively, plotted against the c-parameter. Its zeros correspond to the intersection points of these pathways with the indicated curves h_i.

Poincaré return maps on 2D cross sections computed at these points. Note that these maps contrast significantly from one at the primary hub H_{11} [Fig. 3(a)], as they include 2, 3, and 4 components, correspondingly, on the right-hand side.

Next, we parameterize these 2D maps by 1D ones. To do that, for each 2D return map, we take four points on the curve enveloping the attractor from below and compose the Lagrange polynomial, as previously described in Sec. III. The resulting return maps are shown in the middle row in Fig. 9. One can see that the return map at H_{ii}-hub indeed consists of i parabolas whose far-left point is taken at the repeller O, after one iteration. The dotted lines representing homoclinic obits in these Lamerey (cobweb) diagrams correspond to the homoclinic orbits (bottom row) to the saddle-focus O_1 shown in the phase space of the Rössler model.

It is important to underline another feature of periodicity hubs. In each hub, the separatrix loop to the saddle-focus is maximized in its size so that it becomes the "edge" of the homoclinic attractor [see Figs. 3(b) and 9(a_3)–9(c_3)]. This feature is also documented in the corresponding return maps. Indeed, below H_{ii} on m_i, the left branch of the return map remains lower than the FP O. Above H_{ii}, a newly emerging branch is yet lower than the FP O, so the homoclinic orbit used it only to pass through before landing in the repelling FP at the origin. In contrast, Fig. 10 illustrates the homoclinic attractor with the superimposed homoclinic orbit at the point B on the curve h_1, which is far from forming its edge.

B. Hubs inside the U-shaped h_1-curve

By carefully examining the bi-parameter sweeps, one can observe a hierarchy of secondary hubs (e.g., H_{12}, H_{13}, H_{14}) forming organization centers for shrimp-like stability windows [see Fig. 8(a)]. As was shown in Ref. 41, these secondary hubs lie inside the U-shaped curves h_i corresponding to the primary homoclinic loop. Note that the distinctive U-shape of the bifurcation curves is a common feature of diverse applications with a homoclinic saddle-focus (see, for example, Refs. 50–53, and references therein). In this subsection, we show how return maps can be instrumental in predicting the form of homoclinic loops originating from the most visible secondary hubs located inside the curve h_1.

Let us examine the fragment of h_1 between the curves m_1 and m_2 moving upward along h_1. While searching for the locations of secondary hubs in the diagram [Fig. 8(a)], let us analyze the corresponding return maps, while keeping in mind the vital feature of all hubs, namely, in each hub the homoclinic orbit of the saddle-focus O_1 is *maximized* to "edge" the homoclinic attractor outwardly in the phase space (see Figs. 9 and 11 and contrast them with Fig. 10).

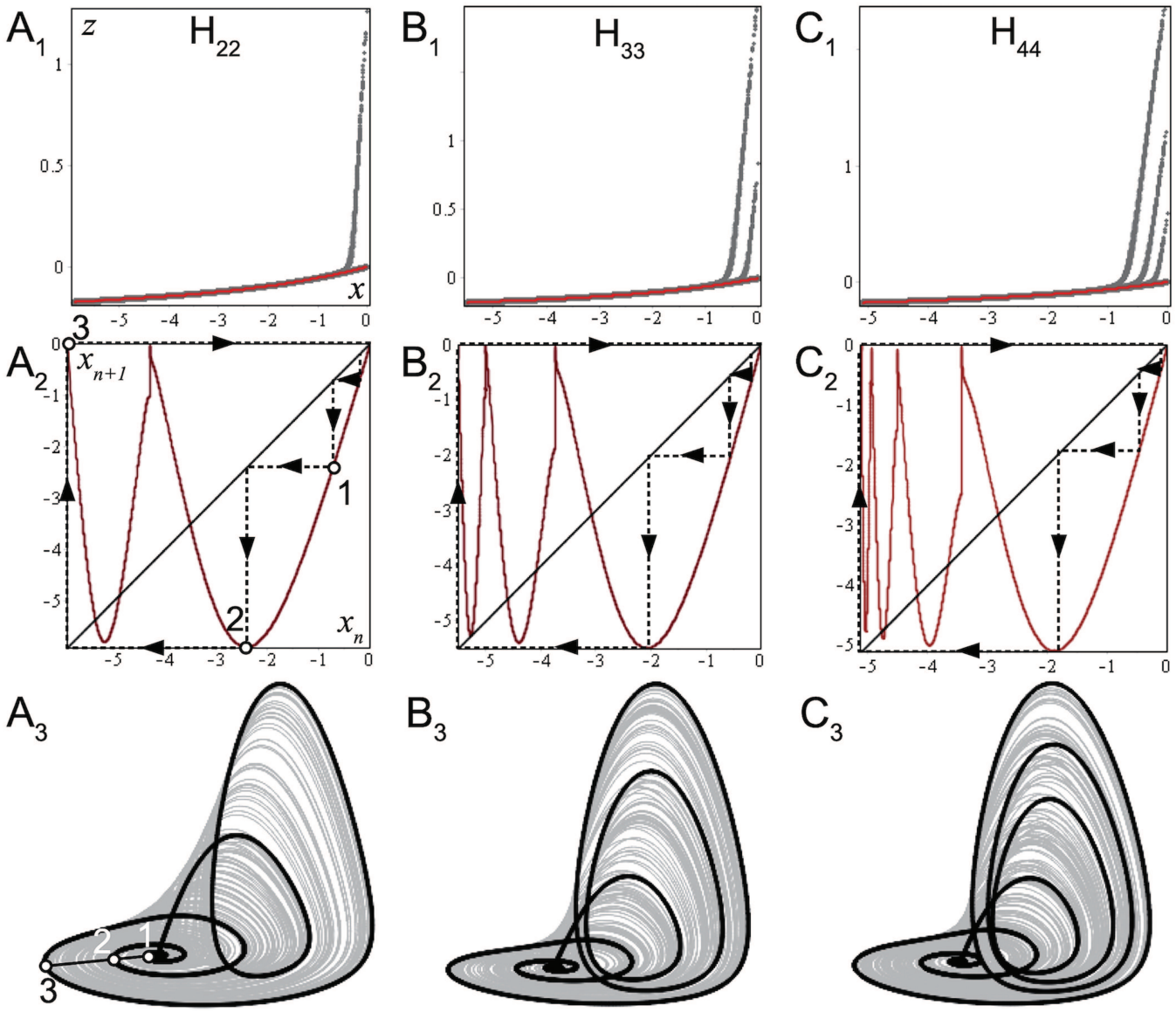

FIG. 9. Homoclinic bifurcations at three primary hubs: (a) H_{22} located at ($c \approx 4.182$, $a \approx 0.4436$), (b) H_{33} at (3.758, 0.4777), and (c) H_{44} around (3.458, 0.4916) [see the bifurcation diagram in Fig. 8(a)]. The corresponding 2D cross sections (top panels), and 1D return maps (middle panels) for h_j-curves with H_{jj}-tuning points reveal multiple branches originating from the saddle-focus O_1 at the top-right corner of the Lamerey (cobweb) diagram (a_2)–(c_2). Bottom panels illustrate the homoclinic orbits demarcating the "edge" of the chaotic attractor.

The hub H_{12} is the most visible secondary hub along the curve h_1 [the largest shrimps are marked with white circles in Fig. 8(a)]. The corresponding return map is presented in Fig. 11(a_1) where the dotted lines represent homoclinic obits. The corresponding homoclinic loop superimposed with the attractor is presented in Fig. 11(a_2). Moving further along the curve h_1, the corresponding return map gains an additional decreasing branch. In the hub H_{13}, the far-left point of this branch matches with the repelling FP O giving birth to a new homoclinic loop, see the corresponding return map with the Lamerey diagrams and phase portrait of the attractor with the homoclinic loop in Figs. 11(b_1) and 11(b_2), respectively. In the H_{14}-hub below the curve m_2, the far-left decreasing branch gives rise to another homoclinic orbit passing on the edge of the attractor [see the corresponding return map with the Lamerey (cobweb) diagram presented in Fig. 11(c_1) and the phase projection of the corresponding homoclinic attractor presented in Fig. 11(c_2)].

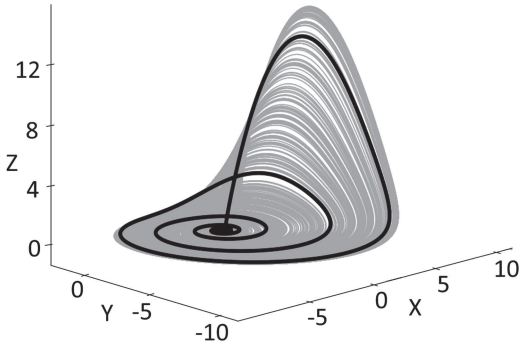

FIG. 10. The separatrix loop of the saddle-focus O_1 at ($c = 4.89$, $a = 0.35$) on the h_1-curve is not fully maximized to edge the homoclinic attractor (shown in the background) (see the contrast with Figs. 9 and 11 for the primary and secondary hubs, respectively).

Above the m_2-curve in the parameter plane, the return map gains an additional increasing branch and then, an additional decreasing one. Moving toward m_3, on the base of these branches, new homoclinic loops appear according to the described scenario. These loops make an additional long passage with respect to the loops associated with the hubs H_{12}, H_{13}, and H_{14}. Moreover, we believe that the same evolution of homoclinic orbits is also observed along all curves h_i corresponding to the primary i-round homoclinic loops.

Finally, we would like to emphasize that each periodicity hub H_{ij} is a fold point for the corresponding homoclinic curve h_{ij}. Each such curve has a U-shape, with two extremely close to each other branches. All these curves reside inside the curve h_i corresponding to the primary i-round homoclinic loop. The possible structure of the corresponding bi-parameter diagrams will be discussed in Sec. VI of this paper.

V. BEYOND THE BOUNDARY OF RÖSSLER ATTRACTOR

This section reveals what the invisible role of the secondary saddle-focus O_2 in the organization of the existence region for observable chaotic attractors in the Rössler model. We will argue that the corresponding demarcation line above which the solutions start running to infinity (Fig. 2) can be well approximated by the curves of homoclinic bifurcations of O_2. The associated bifurcation

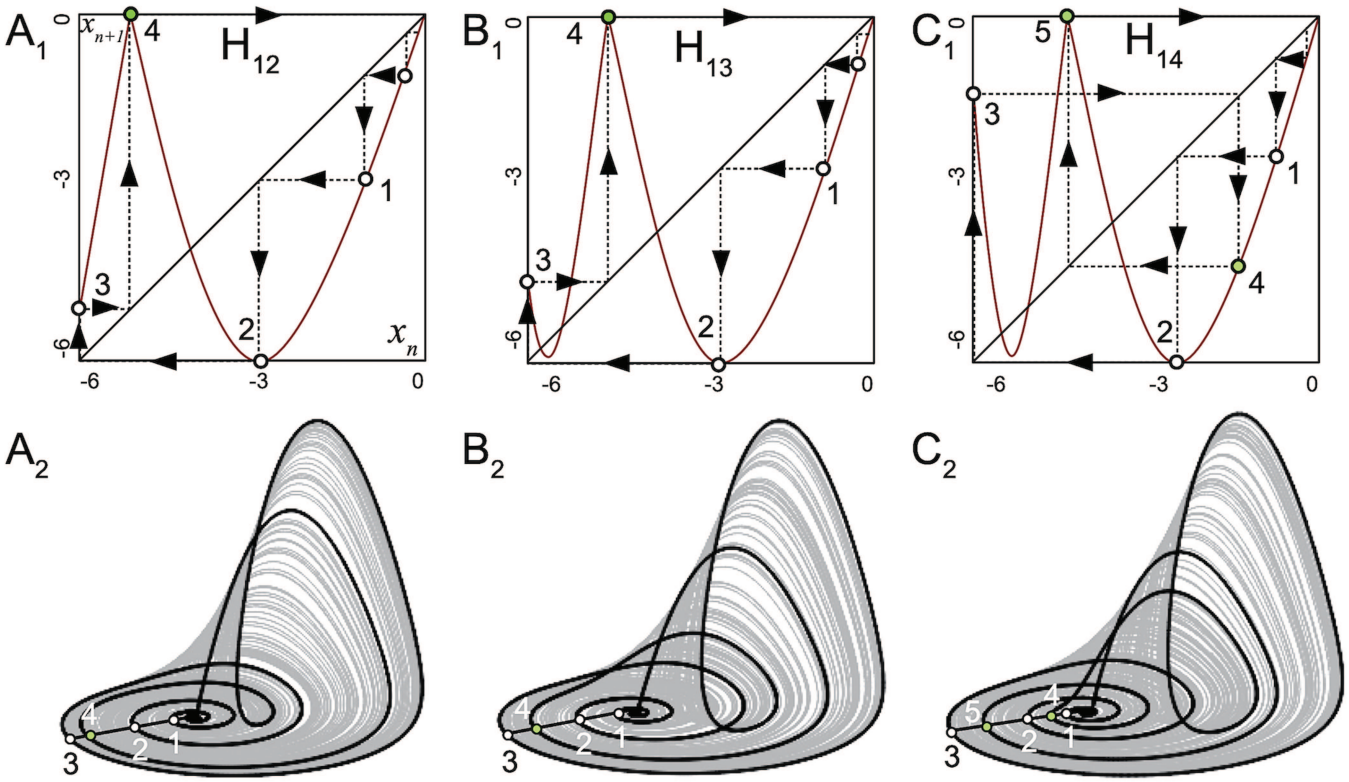

FIG. 11. Homoclinic bifurcations at three secondary hubs: (a) H_{12} located at ($c \approx 4.823$, $a \approx 0.38$); (b) H_{13} at (4.753, 0.4124); and H_{14} near (4.72, 0.4279) [see Fig. 8(a)]. The corresponding return maps depict the homoclinic orbits to the repeller FP O located at the origin and associated with the saddle-focus O_1. Bottom panels depict the homoclinic loops edging the superimposed chaotic attractors.

curves are detected using the simulations combining the symbolic descriptions for homoclinic orbits of O_2 with biparametric sweeps.

It was shown in Sec. I that on the demarcation line, the Rössler attractor merges with the 2D stable manifold W^s of the saddle-focus O_2 of the (2,1)-type (see Fig. 5). Recall that O_2 has two 1D unstable separatrices: W^{u+} fills in the chaotic attractor, while W^{u-} always runs away to infinity. For the parameter values slightly above the demarcation line, the solutions of Eq. (1) start escaping along W^{u-} [see Fig. 2(h)], because the 2D manifold W^s of O_2 no longer shields them. This lets one say that the given crisis of the chaotic attractor is associated with an "infinitely long" homoclinic orbit of the saddle-focus O_2. As there is no way that such long homoclinics can be well computed, so we would limit ourselves to finding shorter homoclinic orbits and corresponding bifurcation curves in the (c, a)-diagram. While sweeping (c, a)-plane, we calculate the number N of global passages (or turns) of W^{u+} around the primary saddle-focus O_1, before it crosses over $W^s(O_2)$ and starts to escape to infinity.

Specifically, for each parameter pair in the sweep, we generate a binary sequence S according to the following algorithm. Whenever the unstable separatrix W^{u+} of O_2 completes a global passage (or a sizable turn) around the equilibrium O_1, the symbol 1 is added to S. After that, there are two options: (i) if W^{u+} makes another turns around O_1, the second symbol 1 is appended to the sequence $S = \{1, 1\}$ and so forth $S = \{1, 1, 1, \dots\}$; and (ii) if W^{u+} runs to infinity, the second symbol is 0 ($S = \{1, 0\}$), and the calculations are halted for these parameter values. The latter case corresponds to the occurrence of the only primary homoclinic orbit of the saddle-focus O_1 [see Fig. 12(a)]. Unlike it, secondary, tertiary and longer homoclinics correspond to multiple bifurcation curves in the parameter plane.

Let us observe that, for example, between any (c, a)-parameter pair corresponding to sequences $\{1, 1, 1\}$ and $\{1, 1, 0\}$, there is always some borderline, read a bifurcation curve, corresponding to the double homoclinic orbits Γ^2_j [see Fig. 12(b)], whereas between sequences $\{1, 1, 1, 1\}$ and $\{1, 1, 1, 0\}$, there exists a triple homoclinic orbit Γ^3_{jk} [see Fig. 12(c)], and so on (the meaning of j and k indices will be explained below).

The pixels of the regions with unitary sequences $S = \{1, 1, \dots, 1\}$ are painted in the yellow color, while regions corresponding to different sequences ending with 0, like $(S = \{1, 1, \dots, 1, 0\})$, are painted in contrast colors depending on the number of 1's in S (see the color bars at the top in Fig. 12 for sequences of length $N = \{2, 3, 4\}$).

We begin our consideration with primary and double homoclinic orbits of the saddle-focus O_2. Figure 13(a) represents the corresponding biparametric sweep in the dedicated region: $2 \le c \le 5$ and $0.45 \le a \le 0.75$. The red-colored region is associated with the same sequence $S = \{1, 0\}$, meaning that the unstable separatrix W^{u+} runs to infinity after a single turn around the saddle-focus O_1. In the

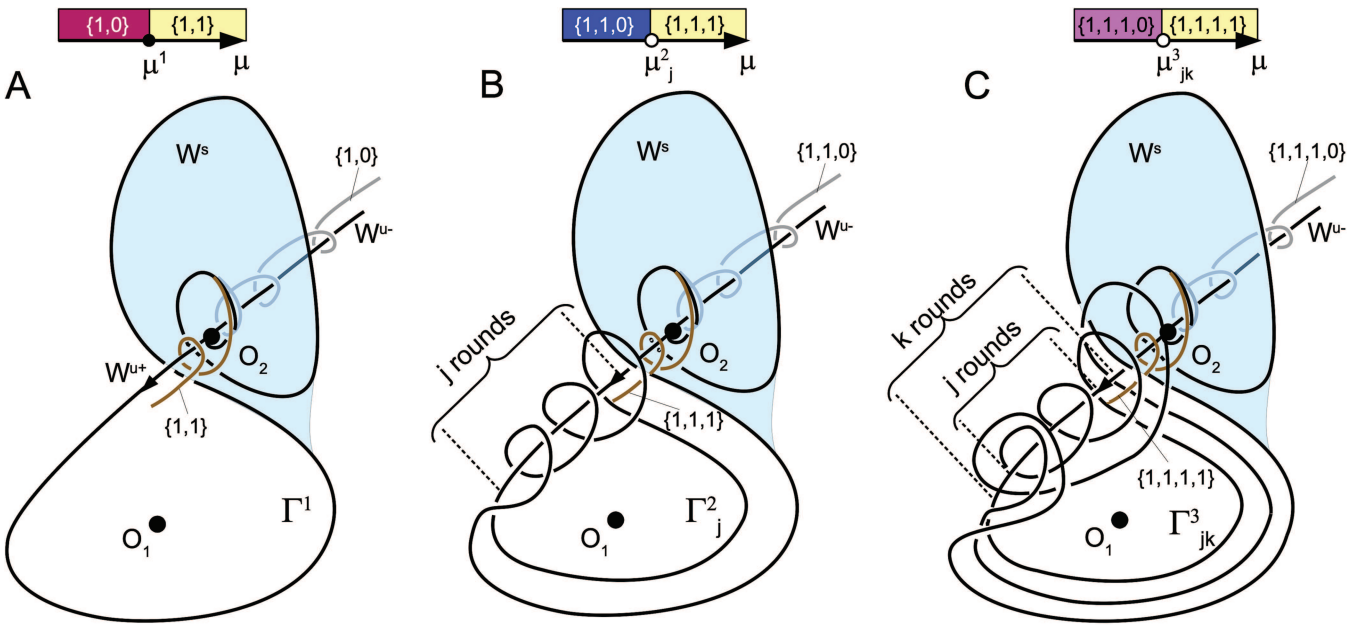

FIG. 12. Geometric idea behind the symbolic algorithm for the detection of homoclinic loops to the saddle-focus O_2 with 2D stable manifold W^s (shown in light blue) and 1D outgoing separatrices: returning W^{u+} and W^{u-} escaping to infinity. (a) Primary homoclinic orbit Γ^1 making a single turn around the saddle-focus O_1 at $\mu = \mu^0 = 0$ (splitting parameter) is coded as {1}, or as {11} if it makes it twice (b), or {111} for three turns in (c), before it runs to infinity alongside W^{u-} with a sequence {1110}. The notions Γ^2_j and Γ^3_{jk} for multiple double and triple homoclinic loops occurring at different values of μ^2_j and μ^2_{jk}, respectively, are used to indicate the number(s) j, k of smaller rounds of W^{u+} on the second and third turns before it returns to O_2. The further the system gets away from the primary loop, the longer the homoclinic orbits Γ^N with increasing index N become, with a greater multiplicity.

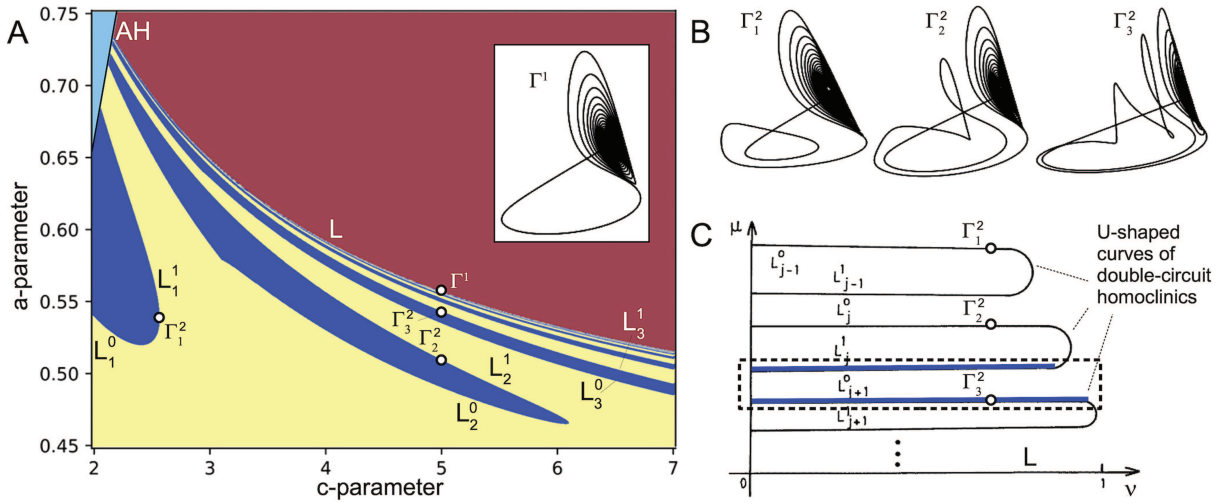

FIG. 13. (a) (c, a)-parameter sweep capitalizing on the symbolic approach with binary sequences up to three symbols long: the red-colored regions is where the 1D unstable separatrix W^{u+} of the saddle-focus O_2 runs to infinity after its first turn around O_1; the corresponding sequence is {1, 0, 0}. The regions in blue and yellow colors correspond to the sequences {1, 1, 0} and {1, 1, 1}, respectively. The borderline L between the red- and yellow-painted regions stands for the primary homoclinic loop Γ^1 of O_2, while boundaries (curves L_j^0 and L_j^1 merging in the some points) between the blue- and yellow-painted regions correspond to double homoclinic loops Γ_j^2, making j-turns around O_2 on the second passage. (b) Homoclinic orbits Γ_1^2, Γ_2^2, and Γ_3^2 with one, two, and three turns around the saddle-focus O_2 at specific points (white dots) in panel A. (c) Bifurcation diagram, courtesy Ref. 51 in the (μ, ρ)-parameter plane (here, μ measures the distance between a saddle-focus and its returning separatrix, and ρ is the saddle-index introduced above). Horizontally stretching U-shaped curves $L_j^{0,1}$ for double homoclinic orbits with increasing j-indices accumulate to the curve L (given by $\mu = 0$) corresponding to primary homoclinic orbit.

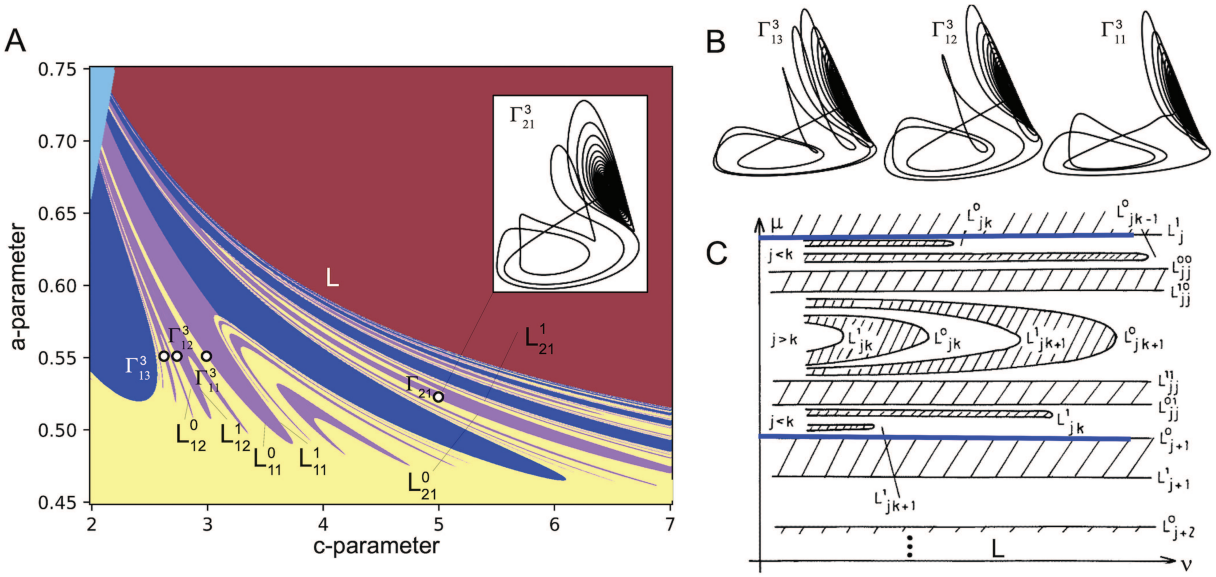

FIG. 14. (a) Biparametric sweep revealing multiplicity of homoclinic orbits to the saddle-focus O_2 and the corresponding binary sequences up to four symbols long. The color scheme is borrowed from Fig. 13: the sequences {1, 1, 1, 0} correspond to the borderlines of the regions painted in the magenta color. The borderlines between the magenta- and yellow-colored regions (curves L_{jk}^0 and L_{jk}^1 bending at folds) correspond to the triple homoclinic loops Γ_{jk}^3 making j-rounds around O_2 on the second turn/passage and k-rounds on the third turn. The boundary between the magenta and blue painted regions is a numerical artifact associated with a transition between double and triple loops, respectively. (b) Triple homoclinic loops Γ_{13}^2, Γ_{12}^2, and Γ_{11}^2 (with 1 round on the first turn and 1, 2, and 3 rounds on the third turn) in the three points marked in panel (a). (c) Schematic diagram (courtesy Ref. 51) revealing self-similar, nested organization of triple homoclinics curves located within a pair of curves L_j^1 and L_{j+1}^0, corresponding to double homoclinics.

blue-colored regions associated with the same sequence $S = \{1, 1, 0\}$, W^{u+} makes two turns around O_1 before escaping. In the yellow-painted region, it makes at least three turns around O_1 to generate the sequence $S = \{1, 1, 1\}$. Hence, the borderline between the red-colored region and the yellow-colored region corresponds to the primary homoclinic orbit Γ^1 of O_2.

The boundaries of the multiple blue-colored regions correspond to the double homoclinic orbits Γ^2_j, where the index j indicates the number of small rounds around the outgoing separatrix W^{u+} of the saddle-focus O_2 on the second turn. As one can see from Fig. 13(a), these bifurcation curves have a U-shaped form.[43] We differentiate their branches with labels L^0_j and L^1_j. It was known from Refs. 43 and 54 that these U-shaped curves corresponding to the double homoclinic orbits accumulate to the primary bifurcation curve L, according to Ref. 51 [see Fig. 13(c)]. The closer these curves approach to L, the greater the index j becomes. One can see from the symbolic sweep presented in Fig. 13 that this agrees well with the theory. A few double homoclinic orbits Γ^1_j are sampled in Fig. 13(b) for the indicated points on curves L^1_j, $j \in \{1, 2, 3\}$ in Fig. 13(a).

Note that within the blue-colored regions, the unstable separatrix W^{u+} always escapes to infinity after two turns around O_1. This implies that no other homoclinic bifurcations can populate these regions. However, that is not the case for the yellow-colored region in which triple- and longer homoclinic orbits can occur. Figure 14(a) represents the homoclinic bifurcation diagram for the sequences of length up to four symbols. In it, there are multiple magenta-colored regions associated with the same sequence $S = \{1, 1, 1, 0\}$ that populate the space between the blue-colored regions. Their boundaries, L^0_{jk} and L^1_{jk}, correspond to triple homoclinic orbits Γ^3_{jk}, where the indices j and k stand, respectively, for the numbers of rounds on the second and third turns around O_1.

Bifurcations of triple homoclinic orbits Γ^3_{jk} were studied in Ref. 51. The idea of such a bifurcation unfolding is sketched in Fig. 14(c). In the Rössler model, such bifurcations occur between curves L^0_{j+1} and L^1_j for double homoclinic orbits marked with blue horizontal lines in Fig. 13(c). Depending on the relationship between j and k, these curves can be either of the U-shaped form if $j < k$ (as for the double loops), or of the horseshoe form, if $j > k$.

We would like to point out that specific boundaries between the magenta- and blue-colored regions in the symbolic sweep in Fig. 14(a) are not bifurcation curves. These curves are associated with transformations of double loops to the triple ones due to the integer arithmetics issue.

Three triple homoclinic orbits Γ^3_{jk} are sampled in Fig. 14(b) for the marked parameter values on the curves L^0_{jk}, $j = 1$, $k \in \{1, 2, 3\}$ in the bifurcation diagram in Fig. 14(a).

A. Stitched bifurcation diagram

Figure 15 completing our case study of the Rössler model represents two bifurcation diagrams stitched together into one: the bottom section reveals the bifurcations mostly due to the primary saddle-focus O_1 in the phase space where the model is strongly dissipative and demonstrate various types of attractors, while the top chart includes the bifurcation curves corresponding to homoclinic orbits (up to the symbolic length 6) of the secondary (in some sense

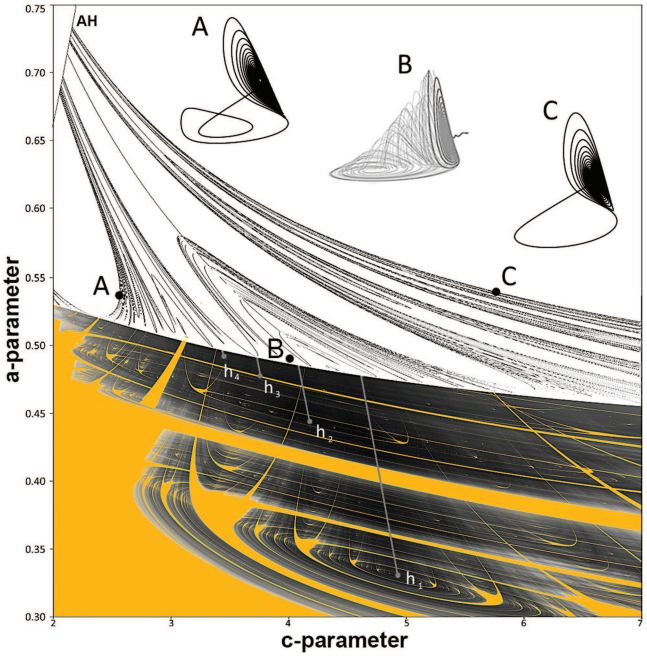

FIG. 15. Stitched (c, a)-bifurcation diagram for the Rössler model. The top b/w chart is due to the primary (top line) and subsequent homoclinics of the saddle-focus O_2 of the (2,1)-type, whose corresponding bifurcation curves terminate on the sub-critical AH-bifurcation curve (that makes O_2 a repeller); the terminal points on the AH-curve represent the cod-2 Belyakov bifurcation nicknamed Shilnikov–Hopf.[44] The bottom part reflects the complex organization of regular and chaotic dynamics stirred up by the primary saddle-focus O_1 of the (1,2)-type.

invisible) saddle-focus O_2 in the phase subspace, with a positive divergence of the vector field. One can see from the stitched diagram that the U-shaped homoclinic curves for O_2 well approximate from above, the demarcation line of the existence region of the Rössler attractors, regardless of whether they are regular or chaotic. For the sake of visual clarity, we did not use the longer homoclinic orbits in this chart.

We underline that without knowing the homoclinic structures due to the secondary saddle-focus O_2, the complete perception of the origin and driving forces of the observable chaotic dynamics in the Rössler model and the metamorphoses of its attractors stirred by the primary saddle-focus O_1 would be barely possible.

VI. h_1-INTERIOR HYPOTHESIS

In this section, we would like to hypothesize about how h_{1j}-curves of the secondary homoclinics of the saddle-focus O_1 can be organized inside the primary bifurcation h_1-curve in the parameter space. The distance ($\sim 10^{-10}$) between the folded branches of h_1 is too infinitesimal to apply implicit computations at this scale, such as the parameter continuation. Furthermore, like any strongly dissipative system, solutions of the Rössler model (1), including 1D separatrices of O_1, while integrated in backward time, become highly

sensitive to the smallest perturbations and tend to escape quickly to infinity in no time.

So, let us try to re-visit and examine further the other, not fully exploited options. Figure 5 is one such example. Recall that the orange spirals in it represent the image of the homoclinic attractor transversely cut through by a 2D cross section. In other words, by construction, spirals flattened in Fig. 16(a) represent the computational point-wise reconstruction of the 2D unstable manifold W^u of the saddle-focus O_1 in the same cross section on which some 2D return map is thereby empirically defined. Note that the intersection(s) of the 1D stable manifold $W^s(O_1)$ is some point(s), which are close to the spirals representing the $W^u(O_1)$-image near the h_1-curve in the parameter space. The primary homoclinic orbit of O_1 emerges when in the 2D return map the $W^s(O_1)$-image—the first intersection point, namely, the p_1-point in Fig. 16(a) touches the spiraling $W^u(O_1)$-image.

Let us make a virtual experiment: locally cross the h_1-curve twice by the following PQ-pathway from the right to the left [see Fig. 16(b)]. By construction, crossing h_1 only, or several h_{1j}-curves (within h_1) along the PQ-pathway in the (c, a)-plane makes the $W^s(O_1)$-image trace down a pq-pathway in the return map as well that crosses twice (in and out) one or consecutively several nested arches of the spiraling $W^u(O_1)$-image. Therefore, the first crossing at the point, p_1, in the return map [Fig. 16(a)] occurs when the h_1-curve is inward-intersected from right to left. The corresponding homoclinic orbit is presented in Fig. 16(c). The second intersection point, p_2, corresponds to the secondary loop occurring on the h_{12}-curve [see Fig. 16(d)], and so forth.

A similar reasoning is also applicable to disclose the structure of the periodicity hubs: whenever the parametric pathway passes right through a hub, then the $W^s(O_1)$-trace (read the pq-pathway) becomes only tangent to some spiral of the $W^u(O_1)$-image in the

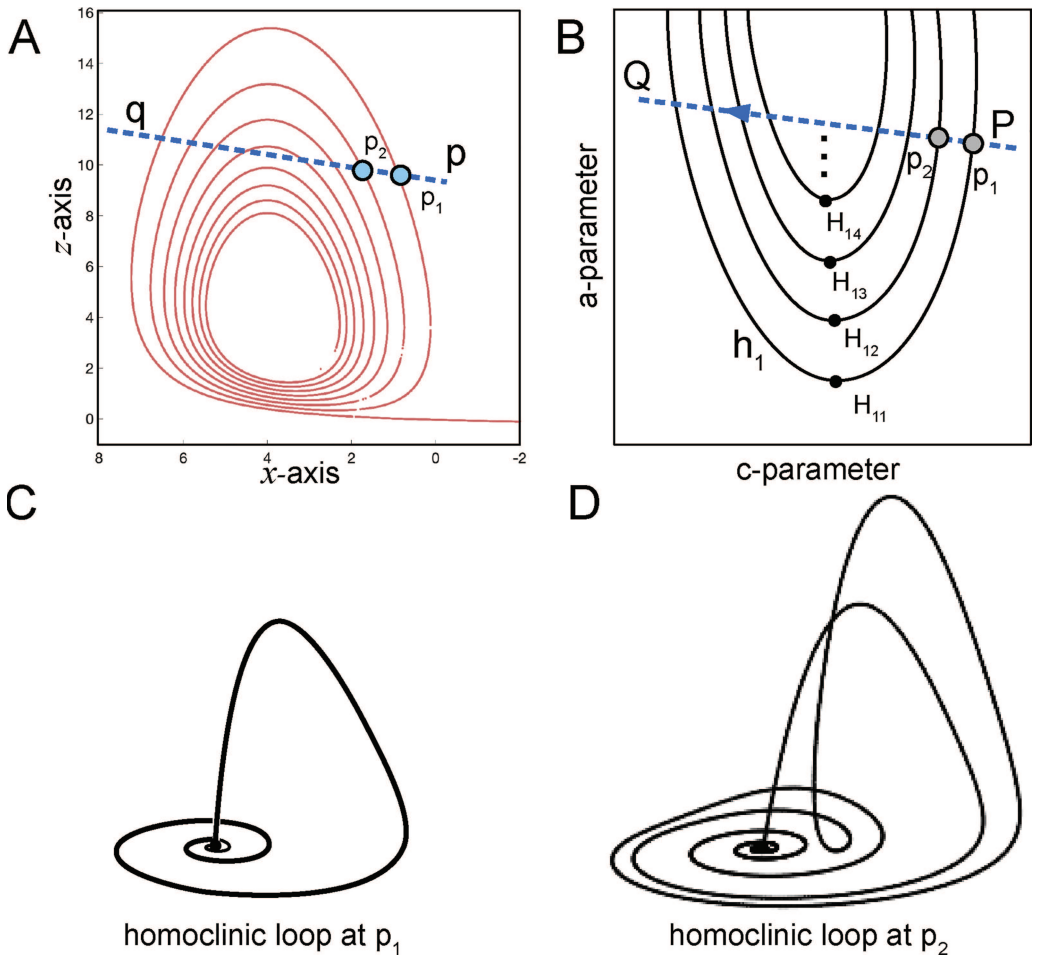

FIG. 16. Inside the h_1-curve. (a) Cross-cut through the multi-funnel attractor in Fig. 5(c) reveals the spirals (orange) being the $W^u(O_1)$-image. Pathway labeled as pq throughout W^u is traced down by the first intersection point of $W^s(O_1)$ with the cross section while following the local PQ-pathway transverse to h_1 in the (c, a)-diagram sketched in panel B. Two crossing points, p_1 and p_2, of the $W^s(O_1)$-image with the $W^u(O_1)$-image represent two homoclinic orbits shown in (c) and (d). (b) Sketch: U-shaped secondary h_{12}, h_{13}, and h_{14}-curves sequentially nested within each other and the primary h_1-curve (see the corresponding homoclinic orbits in Fig. 11).

corresponding return 2D Poincaré map. Now, we can argue to justify a nested organization of the h_{1j}-curves. The assertion is that the $W^s(O_1)$-trace typically (not in hubs) crosses each spiral or arch of the $W^u(O_1)$-image twice. Each pair of such crossing points corresponds to the two branches of each U-shaped h_{1j}-curve nested successfully within a similar outer U-shaped h_{1j-1}-curve, and so forth, as sketched in Fig. 16(b). Let us make it clear again that this is so far our best interpretation of this homoclinic puzzle based upon performed simulations and bifurcation logic. It would be helpful to compare our hypothesis with theoretical and computational findings from other systems featuring periodicity hubs.

VII. CONCLUSION

In this paper, we presented a case study of essential homoclinic bifurcations of two Shilnikov saddle-foci that govern the shape and the intrinsic structure of deterministic chaos observable in the Rössler model. We combine two computational approaches—the first one capitalizing on the use of Poincaré return maps for an interval and the second one utilizing the symbolic description to provide both qualification and quantification of underlying global bifurcations of the strange and periodic attractors in the Rössler model. Specifically, the return map-based approach lets us accurately detect the location of the homoclinic bifurcation curves h_{ij} and their turning points—the so-called periodicity hubs H_{ij} in the parameter space. We would like to underline here that homoclinic chaos, which is directly associated with the Shilnikov saddle-focus O_1, occurs only within extremely narrow domains between the branches of the U-shaped homoclinic bifurcation h_i-curves. While the return maps provide the graphical confirmation of "multi-funnel-ness," we argue that the real cause of the increasing complexity is illustrated for the first time in Fig. 5. It de facto proves that more funnels emerge as the chaotic attractor wraps extra times around the 1D separatrix of the secondary saddle-focus O_2 as both objects get closer.

The symbolic approach based on long transients is the new development in the computational arsenal of nonlinear sciences that aids to identify the regions of chaotic and periodic/regular dynamics in biparametric sweeps. On the other hand, the use of short binary sequences representing the time-progression of the 1D unstable separatrix of the saddle-focus O_2 is a powerful instrument allowing for locating a whole variety of homoclinic bifurcations in biparametric sweeps.

The generality of our computational toolkit makes it universal and applicable to other systems of diverse origins ranging from mathematics through life sciences.

DEDICATION

This paper is dedicated to Otto Rössler on the occasion of his 80th anniversary.

ACKNOWLEDGMENTS

We acknowledge the Brains and Behavior initiative of Georgia State University for the B&B fellowship awarded to K. Pusuluri. We are grateful to D. Turaev and J. Scully for inspiring discussions, as well as H.G.E. Meijer for MatCont tutoring and A.Korotkov for help with finding the curves m_i in Fig. 8. The Shilnikov NeurDS lab acknowledges the NVIDIA Corporation for donating the Tesla K40 GPUs that were actively used in this study. A. Kazakov and A. Shilnikov acknowledge partial funding support from the Laboratory of Dynamical Systems and Applications NRU HSE (Grant No. 075-15-2019-1931) from the Ministry of Science and Higher Education of Russian Federation. Yu. Bakhanova and A. Kazakov acknowledge the RSF (Grant No. 19-71-10048) for the funding support related to the results presented in Secs. IV and VI, and S. Malykh acknowledges the RSF (Grant No. 20-71-10048) for the funding support related to the results presented in Sec. V.

DATA AVAILABILITY

The data that support the findings of this study are openly available in Ref. 55.

REFERENCES

[1] O. E. Rössler, "An equation for continuous chaos," Phys. Lett. A **57**, 397–398 (1976).
[2] O. E. Rössler, "Continuous chaos four prototype equations," Ann. N. Y. Acad. Sci. **316**, 376–392 (1979).
[3] O. Rossler, "An equation for hyperchaos," Phys. Lett. A **71**, 155–157 (1979).
[4] L. P. Shilnikov, "A case of the existence of a denumerable set of periodic motions," Dokl. Akad. Nauk SSSR **160**, 558–561 (1965).
[5] C. Letellier and O. E. Rossler, "Rössler attractor," Scholarpedia **1**, 1721 (2006).
[6] See https://en.wikipedia.org/wiki/Rössler_attractor for more information about "Rossler attractor."
[7] M. Hénon, "A two-dimensional mapping with a strange attractor," in *The Theory of Chaotic Attractors*, edited by B. R. Hunt *et al.* (Springer, 1976), pp. 94–102.
[8] I. Ovsyannikov and L. P. Shilnikov, "On systems with a saddle-focus homoclinic curve," Mat. Sb. **172**, 552–570 (1986).
[9] A. Arneodo, P. Coullet, and C. Tresser, "Oscillators with chaotic behavior: An illustration of a theorem by Shilnikov," J. Stat. Phys. **27**, 171–182 (1982).
[10] D. Turaev and L. P. Shilnikov, "An example of a wild strange attractor," Sb. Math. **189**, 137–160 (1998).
[11] D. Turaev and L. Shilnikov, "Pseudohyperbolicity and the problem of periodic perturbation of Lorenz-like attractors," Dokl. Math. **77**, 23–27 (2008).
[12] V. S. Afraimovich and L. P. Shilnikov, "Strange attractors and quasiattractors," in *Nonlinear Dynamics and Turbulence*, edited by G. I. Barenblatt, G. Iooss, and D. D. Joseph (Pitman, New York, 1983), pp. 1–28.
[13] S. Gonchenko, L. P. Shil'nikov, and D. Turaev, "Quasiattractors and homoclinic tangencies," Comput. Math. Appl. **34**, 195–227 (1997).
[14] S. Gonchenko, A. Kazakov, and D. Turaev, "Wild pseudohyperbolic attractor in a four-dimensional Lorenz system," Nonlinearity (to be published).
[15] A. Lempel and J. Ziv, "On the complexity of finite sequences," IEEE Trans. Inf. Theory **22**, 75–81 (1976).
[16] T. Xing, J. Wojcik, M. A. Zaks, and A. L. Shilnikov, "Fractal parameter space of Lorenz-like attractors: A hierarchical approach," in *Chaos, Information Processing and Paradoxical Games: The Legacy of John S Nicolis* (World Scientific, 2015), pp. 87–104.
[17] T. Xing, R. Barrio, and A. L. Shilnikov, "Symbolic quest into homoclinic chaos," Int. J. Bifurcation Chaos **24**, 1440004 (2014).
[18] R. Barrio, F. Blesa, S. Serrano, T. Xing, and A. L. Shilnikov, "Homoclinic spirals: Theory and numerics," in *Progress and Challenges in Dynamical Systems*, Springer Proceedings in Mathematics & Statistics, Vol. 54 (2013).
[19] K. Pusuluri and A. Shilnikov, "Homoclinic chaos and its organization in a nonlinear optics model," Phys. Rev. E **98**, 040202 (2018).
[20] K. Pusuluri, A. Pikovsky, and A. Shilnikov, "Unraveling the chaos-land and its organization in the Rabinovich system," in *Advances in Dynamics, Patterns, Cognition* (Springer, 2017), pp. 41–60.
[21] K. Pusuluri, H. G. E. Meijer, and A. L. Shilnikov, "Homoclinic puzzles and chaos in a nonlinear laser model," J. Commun. Nonlinear Sci. Numer. Simul. **93**, 105503 (2020).

[22]K. Pusuluri and A. L. Shilnikov, "Symbolic representation of neuronal dynamics," in *Advances on Nonlinear Dynamics of Electronic Systems* (World Scientific, 2019), pp. 97–102.
[23]K. Pusuluri, H. Ju, and A. L. Shilnikov, "Chaotic dynamics in neural systems," in *Encyclopedia of Complexity and Systems Science*, edited by R. A. Meyers (Springer, 2020), pp. 1–13.
[24]K. Pusuluri, "Complex dynamics in dedicated/multifunctional neural networks and chaotic nonlinear systems," Ph.D. thesis (GSU, 2020).
[25]L. P. Shilnikov, "Bifurcation theory and turbulence. I," Methods Qual. Theory Differ. Equations, 150–163 (1986); [L. P. Shilnikov "The theory of bifurcations and turbulence. I," Selecta Math. Sov. **10**, 43–53 (1991)].
[26]O. E. Rössler, "Different types of chaos in two simple differential equations," Z. Naturforsch., A **31**, 1664–1670 (1976).
[27]R. Barrio, F. Blesa, and S. Serrano, "Qualitative analysis of the Rössler equations: Bifurcations of limit cycles and chaotic attractors," Physica D **238**, 1087–1100 (2009).
[28]P. Gaspard, R. Kapral, and G. Nicolis, "Bifurcation phenomena near homoclinic systems: A two-parameter analysis," J. Stat. Phys. **35**, 697–727 (1984).
[29]C. Letellier, P. Dutertre, and B. Maheu, "Unstable periodic orbits and templates of the Rössler system: Toward a systematic topological characterization," Chaos **5**, 271–282 (1995).
[30]S. Fraser and R. Kapral, "Analysis of flow hysteresis by a one-dimensional map," Phys. Rev. A **25**, 3223 (1982).
[31]A. Dhooge, W. Govaerts, Y. A. Kuznetsov, H. G. E. Meijer, and B. Sautois, "New features of the software MatCont for bifurcation analysis of dynamical systems," Math. Comput. Model. Dyn. Syst. **14**, 147–175 (2008).
[32]V. De Witte, W. Govaerts, Y. A. Kuznetsov, and M. Friedman, "Interactive initialization and continuation of homoclinic and heteroclinic orbits in Matlab," ACM Trans. Math. Softw. **38**, 18 (2012).
[33]L. P. Shilnikov, A. L. Shilnikov, D. V. Turaev, and L. O. Chua, *Methods of Qualitative Theory in Nonlinear Dynamics. Parts I and II*, World Scientific Series on Nonlinear Science, Series A Vol. 5 (World Scientific, 1998).
[34]V. S. Afraimovich, S. V. Gonchenko, L. M. Lerman, A. L. Shilnikov, and D. V. Turaev, "Scientific heritage of L.P. Shilnikov," Regul. Chaotic Dyn. **19**, 435–460 (2014).
[35]L. P. Shilnikov and A. L. Shilnikov, "Shilnikov bifurcation," Scholarpedia **2**, 1891 (2007).
[36]N. K. Gavrilov and L. P. Shilnikov, "On three-dimensional dynamical systems close to systems with a structurally unstable homoclinic curve. I," Math. USSR-Sb. **17**, 467 (1972).
[37]N. K. Gavrilov and L. P. Shilnikov, "On three-dimensional dynamical systems close to systems with a structurally unstable homoclinic curve. II," Math. USSR-Sb. **19**, 139 (1973).
[38]R. Barrio, F. Blesa, S. Serrano, and A. L. Shilnikov, "Global organization of spiral structures in biparametric space of dissipative systems with Shilnikov saddle-foci," Phys. Rev. E **84**, 035201 (2011).
[39]C. Bonatto and J. A. Gallas, "Periodicity hub and nested spirals in the phase diagram of a simple resistive circuit," Phys. Rev. Lett. **101**, 054101 (2008).
[40]J. A. Gallas, "The structure of infinite periodic and chaotic hub cascades in phase diagrams of simple autonomous flows," Int. J. Bifurcation Chaos **20**, 197–211 (2010).
[41]R. Vitolo, P. Glendinning, and J. A. Gallas, "Global structure of periodicity hubs in Lyapunov phase diagrams of dissipative flows," Phys. Rev. E **84**(5), 016216 (2011).
[42]L. Belyakov, "Bifurcation set in a system with a homoclinic curve of a saddle," Math. Notes Acad. Sci. USSR **28**(6), 910–916 (1980).
[43]L. Belyakov, "Bifurcation of systems with a homoclinic curve of a saddle-focus with zero saddle value," Math. Notes Acad. Sci. USSR **36**(5), 838–843 (1984).
[44]L. Belyakov, "On one case of the birth of a periodic orbit with homoclinic curves," Math. Notes Acad. Sci. USSR **15**(4), 571–580 (1974).
[45]Y. A. Kuznetsov, O. De Feo, and S. Rinaldi, "Belyakov homoclinic bifurcations in a tritrophic food chain model," SIAM J. Appl. Math. **62**, 462–487 (2001).
[46]Y. V. Bakhanova, A. O. Kazakov, A. G. Korotkov, T. A. Levanova, and G. V. Osipov, "Spiral attractors as the root of a new type of 'bursting activity' in the Rosenzweig–MacArthur model," Eur. Phys. J. Spec. Top. **227**, 959–970 (2018).
[47]A. Kazakov and A. Korotkov, "On spiral chaos of 3D flows," in *Proceedings of the International Conference—School Dynamics, Bifurcation and Chaos* (Lobachevsky State University, 2018), pp. 15–16
[48]A. Gonchenko, S. Gonchenko, and L. P. Shilnikov, "Towards scenarios of chaos appearance in three-dimensional maps," Russ. J. Nonlinear Dyn. **8**, 3–28 (2012).
[49]A. Gonchenko, S. Gonchenko, A. Kazakov, and D. Turaev, "Simple scenarios of onset of chaos in three-dimensional maps," Int. J. Bifurcation Chaos **24**, 1440005 (2014).
[50]O. De Feo, G. M. Maggio, and M. P. Kennedy, "The Colpitts oscillator: Families of periodic solutions and their bifurcations," Int. J. Bifurcation Chaos Appl. Sci. Eng. **10**, 935–958 (2000).
[51]S. V. Gonchenko, D. V. Turaev, P. Gaspard, and G. Nicolis, "Complexity in the bifurcation structure of homoclinic loops to a saddle-focus," Nonlinearity **10**, 409 (1997).
[52]T. Xing, K. Pusuluri, and A. L. Shilnikov, "Ordered intricacy of homoclinics of the L. Shilnikov saddle-focus in symmetric systems," J. Chaos (submitted) (2020).
[53]R. O. Medrano-T., M. S. Baptista, and I. L. Caldas, "Basic structures of the Shilnikov homoclinic bifurcation scenario," Chaos **15**, 033112 (2005).
[54]P. Gaspard, "Generation of a countable set of homoclinic flows through bifurcation," Phys. Lett. A **97**, 1–4 (1983).
[55]See https://bitbucket.org/pusuluri_krishna/deterministicchaosprospector/src/master/ for more information about "Deterministic chaos prospector."